



## Timing of formation of neoglacial landforms in the South Shetland Islands (Antarctic Peninsula): Regional and global implications

David Palacios<sup>a,\*</sup>, Jesus Ruiz-Fernández<sup>b</sup>, Marc Oliva<sup>c</sup>, Nuria Andrés<sup>a</sup>, José M. Fernández-Fernández<sup>a</sup>, Irene Schimmelpfennig<sup>d</sup>, Laëticia Leanni<sup>d</sup>, Benjamín González-Díaz<sup>b</sup>, ASTER Team<sup>d,e</sup>

<sup>a</sup> Department of Geography, Complutense University of Madrid, Spain

<sup>b</sup> Department of Geography, University of Oviedo, Spain

<sup>c</sup> Department of Geography, Universitat de Barcelona, Spain

<sup>d</sup> Aix Marseille Univ, CNRS, IRD, INRAE, Coll France, CEREGE, Aix-en-Provence, France

<sup>e</sup> Consortium: Georges Aumaître, Didier Bourlès, Karim Keddadouche, France

### ARTICLE INFO

#### Article history:

Received 18 November 2019

Received in revised form

18 February 2020

Accepted 26 February 2020

Available online xxx

#### Keywords:

Antarctic peninsula

Byers peninsula

Neoglaciation

Surface exposure dating

### ABSTRACT

The timing of neoglacial advances in the Antarctic Peninsula (AP) is not yet well constrained. Accurate temporal reconstruction of Neoglaciation in the AP is needed to better understand past glacial responses and regional and global teleconnections during the Holocene. Here, we examine all available information about neoglacial advances in the South Shetland Islands (SSI) as well as in the broader geographical context of the AP region and Antarctic continent. In order to shed light on the contrasting chronologies existing for neoglacial advances in these regions, we focused on a case study where a detailed picture of the Holocene deglaciation was already available. Lake sediments revealed that Byers Peninsula, west of Livingston Island (SSI), was fully deglaciated during the Holocene Thermal Maximum. To complement this approach, we identified glacially polished bedrock surfaces, erratic boulders and a moraine ridge near the present front of the glacier in the SE corner. We applied cosmogenic ray exposure (CRE) dating using *in situ* <sup>36</sup>Cl for basalt rocks and <sup>10</sup>Be for granitic rocks in: (i) 8 samples from glacial erratic and ice-rafted boulders, (ii) 2 samples from moraine boulders, (iii) 2 samples from polished bedrock surfaces, and (iv) 1 sample from an erratic boulder deposited on one of these surfaces. The CRE dates indicate that the onset of deglaciation started around  $9.9 \pm 1.2$  ka, with two phases of glacier expansion during the Mid-Late Holocene forming moraines at  $-4.1 \pm 0.5$  and  $-1.0 \pm 0.2$  ka, respectively. The main neoglacial advances in the AP and the SSI were mostly synchronous and coincided with cold periods, as shown by other records (e.g. glacio-isostatic marine terraces, marine and lake sediments). In addition, these periods of glacial expansion show a similar timing to those recorded in the Arctic. These results suggest that Neoglaciation was driven by global climate forcing in both polar areas despite temporal variations at regional and local scale.

© 2020 Published by Elsevier Ltd.

### 1. Introduction

The Antarctic Peninsula (AP; Fig. 1) is affected by intense warming, which is recorded through reliable meteorological measurements since approximately 1950. This most recent period has been called Recent Rapid Warming (RRW), and is characterized by an accelerated temperature increase being four times greater in the

AP region than the Earth's average (Vaughan et al., 2003; Turner et al., 2005). This dramatic temperature rise caused fast melting of glaciers and a generalized retreat of glacier fronts (Vaughan and Doake, 1996; Cook et al., 2005; Kunz et al., 2012; Pritchard et al., 2012). However, since 1998 a tendency towards cooling in the AP and a return to positive mass glacial balances has been detected (Navarro et al., 2013; Engel et al., 2018). This shift is associated with an increase in the frequency of low pressure systems that has led higher precipitation and lower summer temperatures in the region, particularly in the N and NE AP region, including the South Shetland Islands (SSI) (Turner et al., 2016; Sancho et al., 2017; Oliva

\* Corresponding author.

E-mail address: davidp@ghis.ucm.es (D. Palacios).

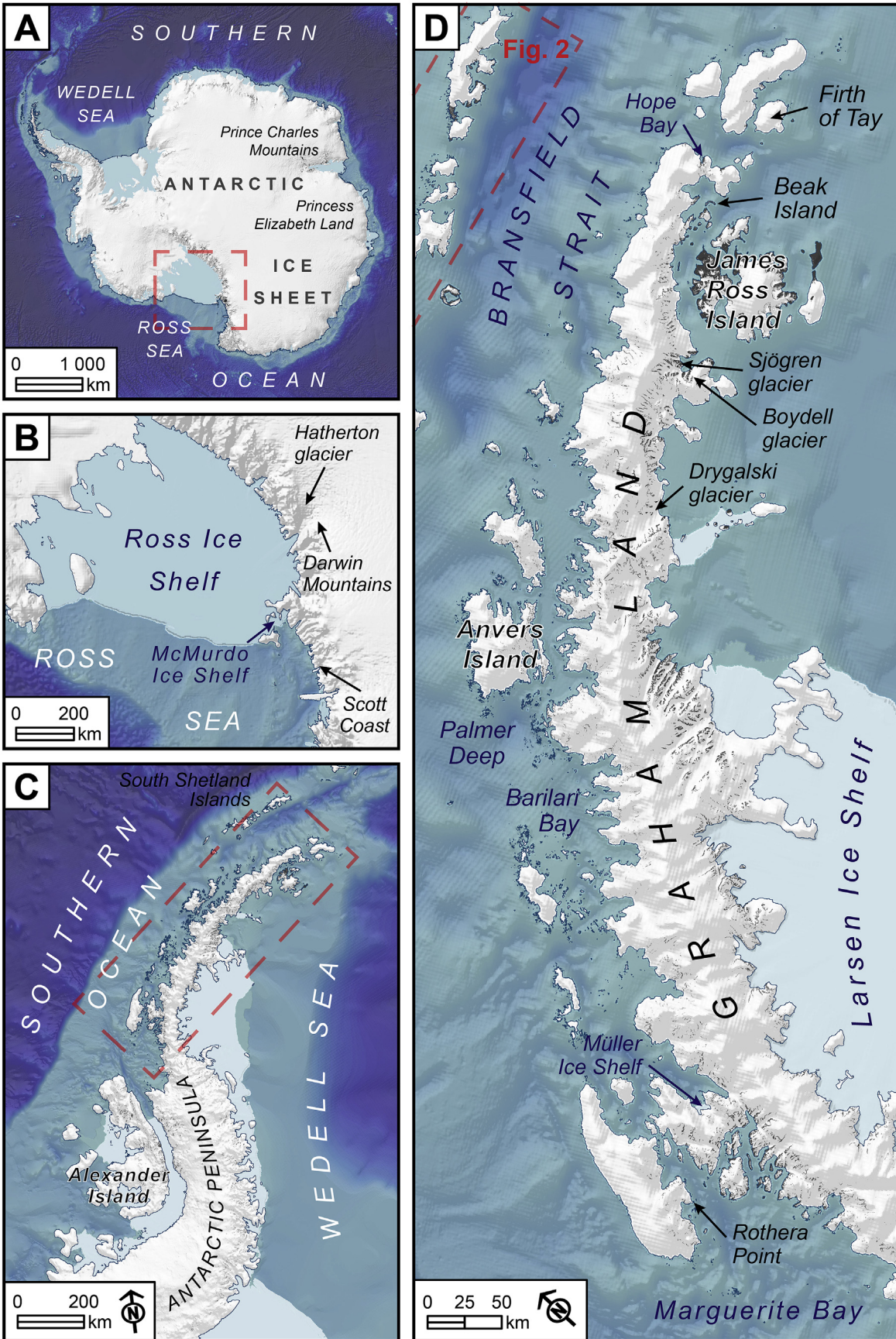


Fig. 1. Location of areas cited in the text related to Antarctica. A) Antarctic Ice Sheet; B) Ross Ice Shelf; C) Antarctic Peninsula; D) Graham Land. This figure is available in colour in the online version.

et al., 2017a) (Fig. 2). Therefore, the question arises whether RRW is the beginning of a trend towards deglaciation in the AP, or a brief warming within the long-term cooling trend affecting this region over the last millennia, continuation of the long-term cooling started since the Neoglaciation (Vaughan et al., 2003; Bentley et al., 2009). However, the timing, distribution, evolution and origin of the neoglaciation advances in the AP region is still poorly understood because of: (i) the lack of historical information on this continent, (ii) the limited number of terrestrial natural archives as sources of palaeoenvironmental information, and (iii) the difficulties of dating these glacial advances in Antarctica (Davies et al., 2012).

Porter and Denton (1967) proposed the generalization of the term Neoglaciation to refer to the glacial advances that occurred after the Holocene Thermal Maximum (HTM: 11–5 ka, Renssen et al., 2009) until the end of the Little Ice Age (LIA). Evidence of Late Holocene glacial advances has been found in a great variety of latitudes and continents (Solomina et al., 2015), widespread also in mountains of the Southern Hemisphere (Clapperton and Sugden, 1988; Porter, 2000) and Antarctica (Clapperton and Sugden, 1988; Clapperton et al., 1989; Ingólfsson et al., 1998). However, delimiting the end of the HTM and the onset of the neoglaciation chronology in the Polar Regions is a matter of great complexity (Kaufman et al., 2004; Renssen et al., 2009, 2012). Similarly, the concept of Neoglaciation in the Arctic has been proposed as a tendency to climate cooling (McKay et al., 2018). However, phases of glacial advances in the Arctic during Neoglaciation alternated with warm periods and glacial retreat, occurring asynchronously across the region without a clear regional pattern (McKay et al., 2018).

As in the Arctic, the chronology of Neoglaciation varied significantly within the AP and throughout the Antarctic continent (Bentley and Hodgson, 2009). According to the available glaciomarine sedimentary records, cold phases during Neoglaciation in the AP region were short, not exceeding 0.5 ka (Yoon et al., 2010), and alternated with longer warm periods (Davies et al., 2012). The first synthesis on climatic and glacial evolution in the AP during the Holocene was carried out by Ingólfsson et al. (1998) who suggested the first neoglaciation advances after 5 ka. Ingólfsson et al. (2003) proposed several other neoglaciation advances between 3 and 1 cal ka BP. Bentley et al. (2009, 2014) reported a generalized warm period in the AP between 4.5 and 2.8 cal ka BP followed by a relatively widespread cold period between 2.5 and 1.2 cal ka BP. Bentley and Hodgson (2009) highlighted that Late Holocene cold phases in different sites across the AP were not synchronous, even in close regions. Hall (2009) provided a synthesis of Holocene glacial evolution for the entire Antarctic continent, including the AP, with many references to neoglaciation landforms. Subsequent studies provided new glacial evidence of neoglaciation landforms in other regions, thus confirming the occurrence of the Neoglaciation as a widespread pattern of glacial advance in the AP (Davies et al., 2012, 2013; Carrivick et al., 2012; Cofaigh et al., 2014). However, these new data also introduce new uncertainties about the time range of neoglaciation phases in different areas across this region (Allen et al., 2010; Davies et al., 2012; Barnard et al., 2014; Cofaigh et al., 2014). The spatio-temporal variations of glacial oscillations over the last centuries are also a consequence of climate variability in the region (Mosley-Thompson et al., 1990; Guglielmin et al., 2016; Brightley, 2017). Recently, Čejka et al. (2019) examined the neoglaciation onset in the AP region through the revision of 22 studies focused on ice cores and marine and lake sediments. They concluded that the beginning of neoglaciation cooling occurred, in average, at  $2.6 \pm 0.8$  cal ka BP, with large spatio-temporal differences within the AP region ranging between 4.8 ka and 1.2 cal ka BP. However, a review on glacier oscillations during Neoglaciation is still missing. Kaplan et al. (2020) provided new information about

the Neoglaciation chronology in the AP and compared it with the neoglaciation advances in Patagonia.

The Byers Peninsula, on the western end of Livingston Island, is the largest deglaciated terrestrial area in the SSI (Fig. 2). In this area, lake records suggest that the retreat of the Rotch Dome Glacier occurred throughout the Holocene (Toro et al., 2013; Oliva et al., 2016; Ruiz-Fernández and Oliva, 2016), although the existence of neoglaciation landforms, such as moraines, is not yet evidenced. The application of cosmogenic radiation exposure (CRE) methods – that have not been applied yet to neoglaciation landforms in the SSI – offers new possibilities to obtain a detailed chronology for the development of these neoglaciation landforms. The knowledge of the age of moraines formed in neoglaciation advances in the Byers Peninsula can provide important information on the possible synchrony of these advances within the context of the AP.

The aim of this paper is to map and date neoglaciation landforms in the SSI as well as explore their paleoclimatic implications in the context of the Antarctic continent. Firstly, we review the current state of knowledge of Neoglaciation in Antarctica, focusing mainly in the AP. In order to provide the most detailed picture on the paleoclimatic evolution in this region, we examined all available records from ice cores, deep marine sediment cores, lake sediments and glacial landforms. Subsequently, we focused on an area of the AP region where information about Holocene glacial advances is still absent: the Byers Peninsula. In this peninsula, we have mapped the spatial distribution of possible neoglaciation moraines, analyzed the geomorphological setting, and applied CRE dating to these landforms.

## 2. The Neoglaciation in the Antarctic Peninsula and South Shetland Islands

A recent synthesis of the evolution of the West and East Antarctic Ice Sheets shows that glacial mass loss was intense from 9 until 7–6 ka in both areas (Mackintosh et al., 2011, 2014), mainly due to ocean warming, although the long-term glacial shrinking had already begun before 10 ka (Larter et al., 2014) (Fig. 1, Table 1). A wide range of climatic proxies provides data on the occurrence of various cold periods in the AP for the last millennia.

In order to constrain the magnitude and the chronology of neoglaciation advances and retreats in the SSI, we first review the climatic evolution over the Mid- and Late Holocene in the AP region based on different environmental sources:

- (i) *Neoglaciation from ice cores in the AP.* Polar ice cores preserve and provide information on climatic changes and their causes, mainly from comparison of the  $\delta^{18}\text{O}$ , deuterium and  $\text{CO}_2$  concentration variations in different layers, as well as on the climate and chronology from the impurities of the ice (Lorius et al., 1990). The most accurate reconstruction from ice core records in the AP comes from James Ross Island, NE AP, which revealed a cold phase between 2.5 and 0.6 cal ka BP, and a peak of cold climate that occurred roughly at 1.4 cal ka BP (Mulvaney et al., 2012; Abram et al., 2013). The last phase of intense cooling was recorded during the LIA at around AD ~1410–1460 (Abram et al., 2013), as also detected in ice cores from other areas in Antarctica, e.g. Ross Sea, with a temperature ca. 2 °C colder than present (Bertler et al., 2011), or in Princess Elizabeth Land, East Antarctica, with a significant cooling at AD 1450–1850 (Li et al., 2009) (Fig. 1 and Table 1).
- (ii) *Neoglaciation from marine sediments in the AP.* Deep marine sediment cores can reveal climatic changes based on the proportion of foraminifera and microfossils that are highly sensitive to sea surface temperatures. The ratio of the oxygen isotopes

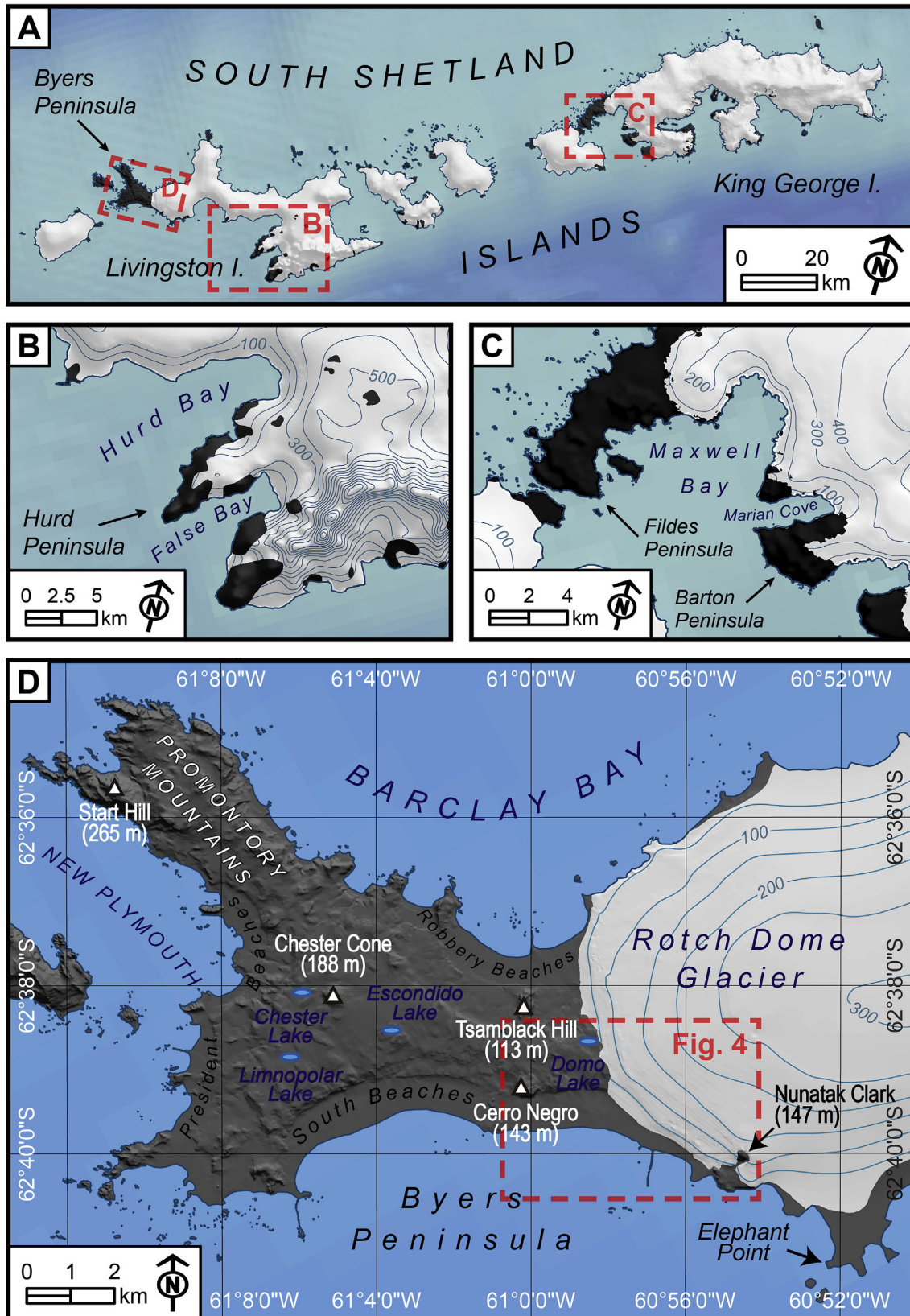


Fig. 2. Location of the areas cited in the text. A) South Shetland Islands; B) Hurd Peninsula; C) Fildes and Barton peninsulas; D) Byers Peninsula. This figure is available in colour in the online version.

**Table 1**  
Timing of neoglaciation advances in the Antarctic Peninsula.

Location	Evidence	Chronology of related events	Neoglaciation environments and landforms	References
James Ross Island	Ice cores	From 2.5 to 0.6 cal ka BP, especially around 1.4 cal ka BP	Cold period	Mulvaney et al. (2012); Abram et al. (2013)
James Ross Island	Lake sediments	At 1.2 cal ka BP	Glacial advance	Björck et al. (1996a, b)
James Ross Island	Glacial landforms	At 6.5, 4.6, 3.9, 2.6 cal ka BP	Glacial advances	Strelin et al. (2006)
James Ross Island	Glacial landforms	At 4.8 ka Be <sup>10</sup>	Glacial advance	Davies et al. (2014)
James Ross Island	Glacial landforms	From 1.5 to 0.3 ka Be <sup>10</sup>	Glacial advances	Davies et al. (2014)
Bransfield Strait	Marine sediments	At 4.5 and 2.5 cal ka BP	Cold periods	Shevenell et al. (2011)
Bransfield Strait	Marine sediments	At 3.5 and 1.2 cal ka BP	Cold periods	Khim et al. (2002); Heroy et al. (2008); Barnard et al. (2014)
Marguerite Bay	Marine sediments	From 2.8 to 0.2 cal ka BP	Cold period	Allen et al. (2010)
Marguerite Bay	Lake sediments	From 2.6/2.0 to 1.1 cal ka BP	Cold periods	Hodgson et al. (2013)
Marguerite Bay	Glacial landforms	At 4.4 ± 0.7 ka Be <sup>10</sup>	Glacial advance	Davies et al. (2017)
Marguerite Bay	Glacial landforms	At 1 ka Be <sup>10</sup>	Formation of ice-cored moraines	Davies et al. (2017)
Palmer Deep	Marine sediments	From 3.3 to 0.1 cal ka BP	Cold period	Domack et al. (2001)
Firth of Tay	Marine sediments	Between 6.0 and 4.5 cal ka BP	Minor glacial advance	Michalchuk et al. (2009)
Firth of Tay	Marine sediments	From 3.5 cal ka BP	General neoglaciation	Michalchuk et al. (2009)
Hope Bay	Lake sediments	Around 5 ka	Glacial advance	Zale and Karlén (1989)
Beak Island	Raised beaches	From 2.9 cal ka BP	Decreased rates of sea level rise associated with neoglaciation events	Roberts et al. (2011)
Scott Coast	Glacial landforms	From 3.5 ka to the LIA	Glacial advances	Hall and Denton (2002)
Anvers Island	Glacial landforms	Until 0.7–0.9 cal ka BP	Glacial advances followed by retreat	Hall et al. (2010)
Sjögren, Boydell and Drygalski glaciers	Glacial landforms	After 1.4 ka	Glacial advances	Balco and Schaefer (2013)
Hatherton Glacier, Darwin Mountains	Glacial landforms	Between 3 and 0.5 ka Be <sup>10</sup>	Formation of moraines	White et al. (2011)
Bransfield Strait	Marine sediments	LIA	Glacial advance	Khim et al. (2002); Barnard et al. (2014)
Müller Ice Shelf	Marine sediments	LIA	Glacial advance	Domack et al. (1995)
Palmer Deep One	Marine sediments	LIA	Glacial advance	Domack et al. (2001)
Barilari Bay, Graham Land	Marine sediments	LIA	Glacial advance	Christ et al. (2015); Reilly et al. (2016)
Hope Bay	Lake sediments	LIA	Glacial advance	Zale and Karlén (1989)
James Ross Island	Glacial landforms	LIA	Glacial advance	Strelin et al. (2006)
Marguerite Bay	Glacial landforms	LIA	Glacial advance	Guglielmin et al. (2016)

from the calcium carbonate shells of foraminifera and coccoliths, and from the silicon dioxide shells of radiolarians and diatoms, is indicative of the temperature of the ocean during the build-up of every shell layer (Rothwell and Rack, 2006). Several sedimentary records were collected from areas adjacent to the AP region. As in ice core records, most records show changes in sedimentation patterns during neoglaciation cold periods, with notable chronological differences. Records obtained in the Bransfield Strait reported abrupt cold conditions at 4.5 and 2.5 cal ka BP (Shevenell et al., 2011), at 3.5 and 1.2 cal ka BP (Khim et al., 2002; Heroy et al., 2008; Barnard et al., 2014) and during the LIA (Khim et al., 2002; Barnard et al., 2014). In other records from the western side of the AP, similar patterns were observed, including long-term cooling trends from 3.3 to 0.1 cal ka BP in Palmer Deep (Domack et al., 2001), from 2.8 to 0.2 cal ka

BP in Marguerite Bay (Allen et al., 2010), and during the LIA in Müller Ice Shelf (Domack et al., 1995) and in Barilari Bay, Graham Land (Christ et al., 2015; Reilly et al., 2016). Neoglaciation cooling was also reported in the NE of the AP, as in the Firth of Tay, where marine sediment cores revealed a minor glacial advance between 6.0 and 4.5 cal ka BP, retreat between 4.5 and 3.5 cal ka BP, and glacial readvance from 3.5 cal ka BP to recent times (Michalchuk et al., 2009) (Fig. 1 and Table 1).

(iii) *Neoglaciation from lake sediments in the AP.* Paleolimnological studies can reveal climatic changes from a wide range of proxies including the analysis of magnetic susceptibility, grain-size distribution, geochemistry, diatoms studies, and geochronology (Zale and Karlén, 1989; Čejka et al., 2019). Čejka et al. (2019) examined the onset of Neoglaciation in the AP region from lacustrine sediments suggesting that it

occurred at 2 cal ka BP, with significant regional variations. Conversely, in our study, we analyzed periods during the Neoglaciation that led to glacial advances. Evidences of neoglaciation advances in the AP from lacustrine sediments suggest a phase of glacial expansion at 1.2 cal ka BP in James Ross Island, (Björck et al., 1996a), at around 5 ka and during the LIA in Hope Bay (Zale and Karlén, 1989) and from 2.6 until 1.1 cal ka BP in Marguerite Bay (Hodgson et al., 2013) (Fig. 1 and Table 1).

- (iv) *Neoglaciation from raised beaches in the AP.* Rates of glacio-isostatic uplift inferred from the elevation of raised beaches are indicative of the intensity of the deglaciation (Simkins et al., 2013). Hall and Denton (1999) determined that these rates were especially high between 8 and 5 cal ka BP in the Ross Sea, suggesting that glacial shrinking decreased during the Mid Holocene. However, decreasing uplift rates can be also indicative of glacial advances (Simkins et al., 2013). In Beak Island, NE AP, the relative sea level fell from a maximum uplift rate of 3.91 mm yr<sup>-1</sup> at around 8 cal ka BP to 2.11 mm yr<sup>-1</sup> between 6.9 and 2.9 cal ka BP, 1.63 mm yr<sup>-1</sup> between 2.9 and 1.8 cal ka BP, and finally to 0.29 mm yr<sup>-1</sup> during the last 1.8 ka BP. This reveals a trend towards more glacial stability and/or glacial readvances during the neoglaciation period (Roberts et al., 2011) (Fig. 1 and Table 1).
- (v) *Neoglaciation from glacial landforms in the AP.* Together with these proxies, some studies have focused on the direct dating of neoglaciation landforms in the AP. Radiocarbon dating of unconsolidated glacial sediments demonstrated the occurrence of six neoglaciation advances at 6.5, 4.6, 3.9 cal ka BP, two around 2.6 cal ka BP, as well as glacial expansion during the LIA in James Ross Island (Strelin et al., 2006). This LIA glacial advance has been also detected in the western AP, namely in Rothera Point, Marguerite Bay (Guglielmin et al., 2016) as well as in Anvers Island, where the glacier front was at or behind its present position at 0.7–0.9 cal ka BP (Hall et al., 2010) (Fig. 1 and Table 1). Outside the AP, in the Scott Coast, in Ross Sea, Late Holocene moraines are distributed on dated raised beaches indicating a neoglaciation advance that occurred between 3.5 ka and the LIA (Hall and Denton, 2002).

However, the most reliable approach to date Neoglaciation in the AP is based on the dating of glacial landforms using CRE methods. In James Ross Island, one of the areas with most CRE dates available, deglaciation was intense until 6 ka (Glasser et al., 2014) and neoglaciation advances occurred at ~4.8 ka and from 1.5 to 0.3 ka (<sup>10</sup>Be ages) (Davies et al., 2014). Close to James Ross Island, in Solari Bay, the Sjögren, Boydell and Drygalski glaciers advanced at 1.4 ka (<sup>10</sup>Be ages) (Balco and Schaefer, 2013). Recently, a work focusing on James Ross Island area reported 49 <sup>10</sup>Be ages of Holocene glacial landforms (Kaplan et al., 2020). These results suggest that the major glacial advance following the HTM occurred at ~7–4 ka, with subsequent phases of glacier expansion between 3.9 and 3.6 ka, just after 3 ka, between ~2.4 and ~1 ka, and from ~0.3 to ~0.1 ka (Kaplan et al., 2020).

Using CRE dating, neoglaciation advances were also detected in the western AP region, as in Alexander Island, Marguerite Bay, where a period of glacial expansion took place at 4.4 ± 0.7 and 1 ka (<sup>10</sup>Be ages) (Davies et al., 2017). Neoglaciation advances have been reported in other areas in Antarctica, such as in the Darwin Mountains between 3 and 0.5 ka (<sup>10</sup>Be ages) (Storey et al., 2010) (Fig. 1 and Table 1).

- (vi) *Neoglaciation in the South Shetland Islands.* The SSI archipelago, located NW of the AP, lies at 120 km from the AP. The

existence of neoglaciation landforms in the SSI is known since the last third of the 20th century (Fig. 2 and Table 2). In the first geomorphological studies, at the end of the 1960s and early 1970s, researchers focused on the existence of moraines distributed a few hundred meters away from the present-day glacier fronts, which transgressed and overlapped recent raised beaches (Arya and Hervé, 1966; Everett, 1971; John and Sugden, 1971; John, 1972; Sugden and John, 1973).

This geomorphological pattern was first described in several deglaciated areas of the SSI, such as Byers and Hurd peninsulas (Livingston Island) and Fildes peninsula (King George Island). Since then, attention has been paid to inferring the age of deglaciation of these raised beaches and their relationship with moraines which transgressed them. Previous works considered that the raised beaches formed as a result of glacio-isostatic rebound due to the partial deglaciation of these islands. The existence of moraines distributed on some of these raised beaches suggest that the moraines are chronologically younger than the raised beaches. Radiocarbon dating of organic fragments interbedded in the raised beach provide a minimum age for the formation of the moraine resting on this beach. In Hurd Peninsula, Everett (1971) inferred a phase of glacial expansion that advanced on a raised beach at 10–12 m a.s.l. and a subsequent glacier advance that left a moraine on a raised beach at 4–6 m a.s.l., which was known as the “False Bay event” (Everett, 1971). The application of radiocarbon dating to raised beaches at 4–6 m a.s.l. in Fildes Peninsula yielded an age of 0.4–0.7 cal ka BP. As this level of the raised beach (4–6 m a.s.l.) is frequently occupied by the youngest moraines existing in the SSI, geomorphologists deduced that these moraines were of LIA age (John and Sugden, 1971; John, 1972; Sugden and John, 1973). Subsequently, further radiocarbon dates differentiate between two levels of raised beaches in the SSI that were covered by the last neoglaciation advances: (i) the first one at 6 m a.s.l., (varying locally between 5 and 7.5 m a.s.l.) associated with a 2–3 km glacier readvance dated at the 13th to early 16th centuries A.D., and (ii) another one at 2–3 m a.s.l. associated with a 0.25–1 km glacier readvance at approximately the 15–17th centuries A.D., that in some areas overlapped the previous (Curl, 1980; Sugden and Clapperton, 1986; Clapperton, and Sugden, 1988). Further radiocarbon dates of raised beaches also suggest, at least, two neoglaciation advances between 3 and 1 cal ka BP (Barsch and Mäusbacher, 1986). The application of lichenometric dating to the moraines distributed on the lowest raised beaches in the SSI confirmed that these landforms developed during LIA glacial advances (Birkenmajer, 1981, 1995, 1998) (Fig. 2 and Table 2).

To better understand the relationship between glacial advances and raised beaches transgressed by moraines, a more accurate geomorphological mapping was conducted to determine the altitude and extent of raised beaches in the Byers Peninsula (Arche et al., 1996) and their correlation with those existing in other ice-free areas in this archipelago (Fretwell et al., 2010). The abundance of ice rafted debris of allocthonous lithology on raised beaches dated between 0.25 and 1.7 cal ka BP suggest that these beaches were related to cold periods of increased glacial extent and greater iceberg delivery (Hall and Perry, 2004). In addition, the dating of the highest raised beaches (located at about 16–20 m a.s.l.) indicates that the most massive deglaciation phase in this peninsula occurred between 9 and 6 cal ka BP, with glaciers close to their current position by 5.5 cal ka BP (Barsch and Mäusbacher, 1986; Mäusbacher, 1991; Del Valle et al., 2002; Hall, 2003, 2010; Bentley et al., 2005; Watcham et al., 2011).

New records obtained during the early 21st century have

**Table 2**  
Timing of the end of deglaciation and geomorphic evidence of neoglaciation advances in the South Shetland Islands.

Location	Chronology of related events	Neoglaciation environments and landforms	References
Several raised beaches in Livingston and King George islands	At 5.5 cal ka BP	Raised beaches distributed at about 16–20 m a.s.l. indicate that the glaciers were close to their current position at that time	Barsch and Mäusbacher (1986); Mäusbacher (1991); Del Valle et al. (2002); Hall (2003); Bentley et al. (2005); Hall (2010); Watcham et al. (2011)
Several lakes in Livingston and King George islands	At 4–5 cal ka BP	Total deglaciation and glaciers close to their current position	Mäusbacher et al. (1989); Björck et al. (1991), 1993, 1996b
Maxwell Bay (King George Island)	Around 5.9 cal ka BP	Deglaciation was completed	Simms et al. (2011a)
Maxwell Bay (King George Island)	From 5.9 cal ka BP	Gradual cooling and more extensive sea-ice cover in the bay	Milliken et al. (2009)
Maxwell Bay (King George Island)	Until 1.7 ka	Neoglaciation advance	Simms et al. (2011a)
Several areas in King George Island	13–17th centuries	Occurrence of two glacial advances: (i) a 2–3 km long advance was dated at the 13th to early 15th CE related to the raised beach 6 m a.s.l., (ii) and another smaller glacial expansion of 0.25–1 km at the 16–17th CE related to raised beach 2–3 m a.s.l.	Curl (1980); Sugden and Clapperton (1986); Clapperton, and Sugden (1988); Birkenmajer (1981), 1995; 1998
Fildes Peninsula (King George Island)	16–18th centuries AD, OSL ages	Moraine associated with the development of the raised beach 4–6 m a.s.l.	Simms et al. (2011a), 2012
Fildes Peninsula (King George Island)	At 0.65 cal ka BP, but possible older advances occurred from 2.8 cal ka BP onwards	Moraine associated with the development of the raised beach 4–6 m a.s.l.	Hall (2007); Hall (2010)
Fildes Peninsula (King George Island)	From 5.8 to 4.8 cal ka BP	Cold period	Chu et al. (2017)
Fildes Peninsula (King George Island)	From 2.7 cal ka BP	Beginning of neoglaciation advances	Chu et al. (2017)
Byers and Fildes peninsulas	From 3 to 1.5 cal ka BP	Two glacial advances	Barsch and Mäusbacher (1986)
Byers and Fildes peninsulas	At 0.4–0.7 cal ka BP	Glacial advances associated with the development of the raised beach 4–6 m a.s.l.	John and Sugden (1971); John (1972); Sugden and John (1973)
Hurd Peninsula (Livingston Island)	Middle and Late Holocene	Two glacial advances related to raised beach 10–12 m a.s.l. and 4–6 m a.s.l.	Everett (1971)
Byers Peninsula (Livingston Island)	At 5.9 cal ka BP	Deglaciation of the central plateau	Toro et al. (2013); Oliva et al. (2016)
Byers Peninsula (Livingston Island)	From 1.7 to 0.25 cal ka BP	Cold periods of increased glacial extent and greater iceberg delivery	Hall and Perry (2004)
Byers Peninsula (Livingston Island)	Between 1.5 and 0.5 cal ka BP	Cold period	Björck et al. (1991)
Byers Peninsula (Livingston Island)	Around 1.8 cal ka BP	Deglaciation of the area close to the present glacial front of Dome Roch glacier	Oliva et al. (2016)

improved our knowledge on the age of moraines in the SSI (Fig. 2 and Table 2). The oldest moraines in Livingston Island identified by Everett (1971) were dated at >7.3 ka, predating the formation of the oldest raised beaches (Sugden and John, 1973; Curl, 1980; López-Martínez et al., 1992; Hall and Perry, 2004; Bentley et al., 2005; Hall, 2009; Fretwell et al., 2010). Hall (2007) dated by radiocarbon the youngest moraines previously studied in Fildes and Hurd Peninsulas (Everett, 1971; John and Sugden, 1971; John, 1972; Sugden and John, 1973). However, Hall (2007) considers the possibility that there could have been previous advances as old as 2.8 cal ka BP. Radiocarbon ages from a 4–6 m raised beach related to these moraines support glacial advance and transgression during the LIA. The application of Optically Stimulated Luminescence (OSL) dating methods to these younger beaches at 4–6 m in the Fildes Peninsula confirmed an age of the 16–18th centuries AD, which coincided with the LIA (Simms et al., 2011a, 2012).

On the one hand, at the end of the 80s and beginning of the 90s, sediment cores collected from several lakes in Livingston and King George Islands reported radiocarbon minimum ages of 4–5 cal ka BP for deglaciation (Mäusbacher et al., 1989; Björck et al., 1991, 1993, 1996b). The analysis of lake sediments from a number of lakes in the western part of the Byers Peninsula suggested the occurrence of a warm period occurring between 3.2 and 2.7 cal ka BP (Björck et al., 1993) and a remarkable cooling between 1.5 and 0.5 cal ka

BP (Björck et al., 1991). More recent studies suggest that the onset of the deglaciation of the Byers Peninsula occurred at 8.3 cal ka BP (Toro et al., 2013), with the deglaciation of the central plateau taking place between 8.3 and 5.9 cal ka BP and ice-free exposure of the easternmost fringe, close to the present-day glacier front, around 1.8 cal ka BP (Oliva et al., 2016).

CRE dating methods were applied to polished bedrock surfaces in the Barton Peninsula (King George Island) along a transect from the highest peaks to the coast. These data showed that deglaciation of this small peninsula had begun earlier than inferred from lake sediments and raised beaches, between 17 and 14 ka, and had finished 1 ka ago (Seong et al., 2009). Hall (2009) CRE dated moraines from Hurd Peninsula and Marion Cove (King George Island) at 1.5–1.0 ka (Hall and Stone, personal communication).

Finally, the analysis of marine sediments in Maxwell Bay (King George Island) determined that there was rapid glacial retreat from 10.1 to 8.2 cal ka BP and a period of gradual cooling and more extensive sea-ice cover in the bay from 5.9 cal ka BP onwards, with no evidence of LIA glacial advance (Milliken et al., 2009). However, a more recent study of marine sediments in Maxwell Bay confirmed that the deglaciation began as soon as 14 cal ka BP – as was proposed by CRE dating in the nearby Barton Peninsula (Seong et al., 2009) – and that deglaciation was completed by 5.9 cal ka BP, with a neoglaciation advance into the bay ending at approximately 1.7

ka (Simms et al., 2011a). Recent coastal sediment analysis in Fildes Peninsula showed a cold period from 5.8 to 4.8 cal ka BP, a mid-Holocene climatic optimum between 4.4 and 2.7 cal ka BP, and the onset of Neoglaciation at 2.7 cal ka BP (Chu et al., 2017). Sediment cores obtained from the continental shelf of the northern SSI pointed to the existence of a cold period around 0.33 cal ka BP, which must have corresponded to the LIA (Yoo et al., 2009).

To sum up, despite varied results, a common pattern can be deduced in studies of neoglacial phases in the SSI in the context of AP region. The glaciers were similar to or smaller than present-day in the AP, as in the SSI, around 6 ka.

Before the warmer period detected in the AP between 4.5 and 2.8 cal ka BP (Bentley et al., 2009), a cold period with the first neoglacial advances occurred around 5 ka in many places of the AP and the rest of the continent (Zale and Karlén, 1989; Mosley-Thompson, 1996; Khim et al., 2002; Strelin et al., 2006; Heroy et al., 2008; Bentley et al., 2009; Michalchuk et al., 2009; Davies et al., 2012, 2017; Shevenell et al., 2011; Carrivick et al., 2012; Cofaigh et al., 2014; Barnard et al., 2014; Kaplan et al., 2020). So far, there is no evidence of this neoglacial advance in the SSI, except perhaps for the references made by Everett (1971) in the Hurd Peninsula about moraines in relation to the raised beaches at 10–12 m a.s.l.

Another period of widespread neoglacial advance took place in the AP between 2.8 and 1.4 ka, with cooling intensifying between 1.8 and 1.4 cal ka BP. (Mosley-Thompson, 1996; Björck et al., 1996a, b; Khim et al., 2002; Heroy et al., 2008; Bentley et al., 2009; Yoon et al., 2010; Domack et al., 2001; Strelin et al., 2006; Michalchuk et al., 2009; Allen et al., 2010; Davies et al., 2012, 2014; Mulvaney et al., 2012; Shevenell et al., 2011; Mulvaney et al., 2012, 2012; Abram et al., 2013; Hodgson et al., 2013; Barnard et al., 2014; Čejka et al., 2019; Kaplan et al., 2020). To date, this glacial advance is also poorly represented in the SSI, with the only reference by Hall (2007, 2009). However, there is some evidence of a cold period around 1.8 ka in the SSI from other paleoclimatic proxies, such as ice rafted debris on raised beaches (Hall and Perry, 2004), lake sediments (Björck et al., 1991, 1993; Oliva et al., 2016), and marine records (Chu et al., 2017).

The information available on glacial advances during the LIA is varied across the AP, as in the SSI. Similarly, there is clear evidence of advances in some areas (Strelin et al., 2006), but it is absent in archives such as lake and marine sediments (Shevenell et al., 2011; Hodgson et al., 2013) as well as in ice core records (Mulvaney et al., 2012; Brightley, 2017). In any case, it is important to note that in

many areas a cooling period was observed from 1.5 ka to the first cooling events associated with the LIA (Zale and Karlén, 1989; Domack et al., 2001; Hall and Denton, 2002; Allen et al., 2010; Storey et al., 2010; Michalchuk et al., 2009; Balco and Schaefer, 2013; Davies et al., 2014, 2017). On the other hand, most of the studies carried out on the youngest moraines of the SSI, transgressing the 4–6 m raised beach, confirmed that they were formed during the LIA, between the 16th and 18th centuries AD, with minor age differences depending on dating methods.

### 3. Geographical setting of the case study: the Byers Peninsula

With the aim of resolving the discrepancies observed between the SSI and the rest of the AP on the timing of development of neoglacial landforms, this work explores the age of formation of several landforms in an area that is already known to have been deglaciated during the Mid-Late Holocene (Oliva et al., 2016), the Byers Peninsula, the largest ice-free area in the SSI (Fig. 2 and Table 3). The Byers Peninsula (62°34'35"–62°40'35"S, 60°54'14"–61°13'07"W) is located on the western end of Livingston Island, the second largest island in the SSI, with an area of approximately 60 km<sup>2</sup>, and a maximum altitude of 265 m a.s.l. The peninsula is part of a Jurassic-Quaternary magmatic forearc generated by Mesozoic and Cenozoic subduction processes along the South Shetland Trench (Smellie et al., 1980; Alfaro et al., 2010). This peninsula is composed of Upper Jurassic-Lower Cretaceous sedimentary deposits (mainly sandstones, mudstones and conglomerates) and volcanic and volcanoclastic rocks, with abundant intrusive igneous rocks of basalt-basaltic andesite composition (Smellie et al., 1980; Hathway and Lomas, 1998; Parica et al., 2007; Alfaro et al., 2010). The geomorphology of the Byers Peninsula (Araya and Hervé, 1966; John and Sugden, 1971; López-Martínez et al., 1996) is formed by a high plateau (80–110 m), considered a marine platform, onto which protruded a series of volcanic plugs such as Start Hill (265 m a.s.l.), Chester Cone (188 m), Cerro Negro (143 m), Tsamblak Hill (113 m) and Clark Nunatak (147 m). Many lakes are distributed on this plateau, such as the Limnopolar, Chester, Escondido, Cerro Negro and Domo lakes (Fig. 2, Table 3). This central plateau is encircled by an intermediate marine platform (50–80 m) that is surrounded by a lower platform above which Holocene raised beaches from 2 to 15–16 m a.s.l. have developed. The sequence of raised beaches is particularly well-preserved in the South beaches (S), the Robbery beaches (N), and the President beaches (W). The ice-free area of the Byers Peninsula

**Table 3**  
End of deglaciation, Neoglacial evidence and related features in the Byers Peninsula.

Location	Evidence	Chronology of related events	Neoglacial environments and landforms	References
From West to East	Lake sediments	From 8.3 to 1.8 cal ka BP	Deglaciation of the entire peninsula	Toro et al. (2013); Oliva et al. (2016)
Front of the Rotch Dome glacier	Geomorphical evidence	LIA?	Ice-cored moraines distributed on the raised beach 4–5 m a.s.l.	John and Sugden (1971); López Martínez et al., 1996.
Domo Lake	Lake sediments	Slightly younger than 1.8 cal ka BP	Deglaciation of the lake	Oliva et al. (2016)
Midge Lake	Lake sediments	Between 1.5 and 0.5 cal ka BP	Cold periods	Björck et al. (1991)
Southern Beaches	Raised beaches	1.8 cal ka BP	Raised beach 10 m a.s.l.	Hansom (1979)
Southern Beaches	Raised beaches	15–17th centuries CE	Raised beach 6 m a.s.l.	Curl (1980)
Southern Beaches	Raised beaches	1.7 cal ka BP	Raised beach 6 and 10 m a.s.l. with ice rafted debris	Hall and Perry (2004)
Southern Beaches	Raised beaches	From 7.4 cal ka BP to 15–17th centuries CE	Raised beaches from 15 to 6 m a.s.l.	Hall (2003), 2010
West front of the Rotch Dome glacier	Aerial imagery	From 1971	Stable ice-cored moraines	John and Sugden (1971); López Martínez et al., 1996; Hall (2010)
South front of the Rotch Dome glacier	Aerial imagery	From 1956 to 2000	Retreat of ice-cored moraines	Oliva and Ruiz-Fernández (2015), 2017

is delimited in its eastern flank by the Dome Rotch Glacier, which covers the rest of the western part of Livingston Island reaching a maximum altitude of 360 m. Although there is no information about the recent evolution of Dome Rotch Glacier in the side of the Byers Peninsula, significant retreat has been observed in other neighbouring coastal fringes since the 1950s (Birkenmajer, 2002) that seems to have decelerated in the last decade (Navarro et al., 2013; Oliva et al., 2017a, b).

The mean annual temperature is around  $-2.8$  °C at 80 m and annual precipitation (rain and snowfall) reaches ca. 650 mm at this altitude (Bañón et al., 2013; De Pablo et al., 2014). Discontinuous permafrost patches have been detected in raised beaches (Correia et al., 2017) whereas permafrost is continuous at the central plateau (De Pablo et al., 2014). Abundant periglacial landforms distributed across the peninsula show evidence of active periglacial dynamics in the area, strongly conditioned by local topography and snow distribution (Serrano et al., 1996; López-Martínez et al., 2012; Hrbáček et al., 2016; Ruiz-Fernández et al., 2016; Oliva et al., 2017b). Most of the area is covered by bryophytes and lichens, including the two native Antarctic phanerogams on the raised beaches (Lindsay, 1971; Vera, 2013), which makes the Byers Peninsula a unique environment in terms of terrestrial biodiversity within Antarctica (Benayas et al., 2013). To protect this hotspot of biodiversity, the Byers Peninsula was designated an Antarctic Specially Protected Area (ASPA N° 126).

The Byers Peninsula was covered by an ice sheet distributed across the SSI during the last glacial cycle (Araya and Hervé, 1966; John and Sugden, 1971; López Martínez et al., 1996). This ice sheet was connected with the AP ice sheet during the maximum ice extent, though it became isolated as ice started thinning during the deglaciation (Cofaigh et al., 2014). Previous studies on lake sediments have determined that the deglaciation of the Byers Peninsula occurred from W to E, with a timing of 7.5 to 1.8 cal ka BP (Toro et al., 2013; Oliva et al., 2016; Ruiz-Fernández and Oliva, 2016). Domo Lake, located only at 350 m from the present glacier front, was deglaciated around 1.8 ka (Oliva et al., 2016). Several geomorphological landforms and deposits of glacial origin are distributed between the contemporary glacial front and the sea. This is the case of the large longitudinal ice-cored moraines located in front of the Rotch Dome Glacier (Martínez De Pisón et al., 1996; Ruiz-Fernández et al., 2016). John and Sugden (1971) observed how these moraines override all marine levels incorporating littoral deposits; they suggested that the most recent moraines were directly related to the 4–6 m beach and were contemporary in age, representing thus a recent glacial readvance. Hansom (1979) radiocarbon dated a 10 m a.s.l. raised beach at 1.8 cal ka BP, whereas Curl (1980) reported that the 6 m a.s.l. raised beach formed during the 15–17th centuries AD. Hall and Perry (2004) suggested that this beach and the 10 m a.s.l. unit formed during cold periods over the last 1.7 cal ka BP, as they are rich in ice rafted debris. Hall (2003, 2010) contributed numerous dates for all the sequences of raised beaches in the main complexes of the Byers Peninsula, concluding that the highest levels formed at 7.4 cal ka BP and confirming that the 6 m a.s.l. raised beach developed during the 15–17th centuries AD. The frontal ice-cored moraines in front of the Rotch Dome Glacier have been very stable over the last decades, as can be seen in photos and descriptions in old publications (John and Sugden, 1971; López Martínez et al., 1996; Hall, 2010). The glacier has retreated from these moraines only in the vicinity of the northern coast and in the southern fringe, around Clark Nunatak (Martínez De Pisón et al., 1996). In the nearby peninsula of Elephant Point, only 3 km SE of Clark Nunatak, a similar retreat occurred from 1956 to 2000 (Oliva and Ruiz-Fernández, 2015, 2017) (Fig. 2 and Table 3).

## 4. Methodology

### 4.1. Geomorphological research and sampling strategy

In the eastern fringe of the Byers Peninsula, next to Rotch Dome Glacier, an ice-cored moraine has been described to be in contact with the glacier front from 1966 to 1996 (Araya and Hervé, 1966; John and Sugden, 1971; Martínez De Pisón et al., 1996) (Fig. 2). Over these thirty years, the limits, extent, and shape of the ice-cored moraine crests were identical to those described in earlier observations (Martínez De Pisón et al., 1996), showing evidence of the prevailing geomorphic stability at annual to decadal timescales (López Martínez et al., 1996; Hall, 2010). The ice-cored moraine system develops from a single polygenic ridge in the southern edge to a sequence of twelve ridges in its northern fringe next to Robbery beaches (Ruiz-Fernández et al., 2016). These ice-cored moraines are similar to those described in other areas of the AP region (Hambrey et al., 2015). As for Hurd and Fildes peninsulas, Martínez de Pisón et al. (1996) proposed also a synchronicity between the timing of formation of raised beaches and moraines in the Byers Peninsula.

The objective of the geomorphological research was to explore the existence of moraines disconnected from the glacier front of the Roch Dome Glacier, which would suggest the occurrence of neoglacial advances. Roch Dome Glacier moraines include sediments transported by the glacier from the interior of the island, and, therefore, are mostly composed of basalts. We sampled some of these moraine boulders to apply CRE dating using *in situ*  $^{36}\text{Cl}$ . These moraines transgressed raised beaches whose age is already well constrained (Hall, 2003, 2010) and provide a minimum age for the development of the moraines that lay on them. In addition, researchers already identified the existence of ice-rafted granite boulders on these raised beaches (Hall and Perry, 2004). These boulders were sampled to be dated using the *in situ*-produced  $^{10}\text{Be}$  dating method to study their possible chronological relationship with the sampled moraine. Finally, we collected samples from glacially polished bedrock surfaces close to the present glacier front for  $^{36}\text{Cl}$  dating in order to date the glacier retreated from this position.

### 4.2. CRE sampling and analytical procedures

During the fieldwork campaign, a total of 12 samples were taken from glacially polished outcrops and >1-m-diameter erratic/moraine boulders by means of hammer and chisel. We focused on flat gentle surfaces on the top of the boulders/outcrops and avoided steep surfaces and sharp crests in order to ensure the optimal cosmic-ray flux reception. We selected the most stable boulders, which were rooted in the moraines, with no signs of spalling or fracturing and that could not have been deposited through gravitational processes from rock walls. The thickness of the samples ranged from 1.8 to 4.5 cm (Table 4). Following the sample collection, they were crushed and sieved to the 0.25–1 mm fraction at the “Physical Geography Laboratory” of the Complutense University of Madrid. Then the samples were physically and chemically processed at the “Laboratoire National des Nucléides Cosmogéniques” (LN2C) of the “Centre Européen de Recherche et d’Enseignement des Géosciences de l’Environnement” (CEREGE, Aix-en-Provence, France). As the sampled surfaces were constituted both by basaltic and granitic rocks (Table 4), samples were processed for measurement of the *in situ* cosmogenic nuclides  $^{36}\text{Cl}$  (10 samples) and  $^{10}\text{Be}$  (2 samples) by accelerator mass spectrometry (AMS), respectively.

In the case of the  $^{36}\text{Cl}$ , the sample preparation procedures were similar to those described in Schimmelpfennig et al. (2011).

**Table 4**  
Geographic location of samples, topographic shielding factor, sample thickness and distance from terminus.

Sample name	Geomorphological unit	Landform	Latitude (DD)	Longitude (DD)	Elevation (m a.s.l.)	Topographic shielding factor	Thickness (cm)	Dist. from present moraine ridge	Isotope
BYC-1	Deglaciated bedrock	Glacially-polished surface	-62.6731	-60.9199	28	0.9961	1.8	600	<sup>36</sup> Cl
BYC-2	Deglaciated bedrock	Glacially-polished surface	-62.6705	-60.9223	47	0.9995	4.8	350	<sup>36</sup> Cl
BYC-3	Deglaciated bedrock	Erratic boulder	-62.6707	-60.9223	47	0.9912	4.0	350	<sup>36</sup> Cl
BYC-4	Moraine (nunatak Clark, W)	Moraine boulder	-62.6716	-60.9163	36	0.9963	4.5	–	<sup>36</sup> Cl
BYC-5	Moraine (nunatak Clark, W)	Moraine boulder	-62.6704	-60.9166	35	0.9956	3.5	–	<sup>36</sup> Cl
BYC-9	Raised beach (+10/12 m)	Erratic boulder	-62.6654	-60.9409	11	0.9992	3.0	200	<sup>36</sup> Cl
BYC-10	Raised beach (+10/12 m)	Erratic boulder	-62.6660	-60.9386	10	0.9992	2.0	200	<sup>36</sup> Cl
BYC-11	Raised beach (+10/12 m)	Erratic boulder	-62.6668	-60.9349	10	0.9992	3.1	200	<sup>36</sup> Cl
BYC-12	Raised beach (+10/12 m)	Ice-rafted boulder	-62.6714	-60.9293	4	0.9900	3.5	–	<sup>10</sup> Be
BYC-13	Raised beach (+10 m)	Erratic boulder	-62.6714	-60.9295	5	0.9900	3.2	–	<sup>36</sup> Cl
BYC-14	Raised beach (+10 m)	Erratic boulder	-62.6713	-60.9298	5	0.9900	1.8	–	<sup>36</sup> Cl
BYB-10	Raised beach (+10/12 m)	Ice-rafted boulder	-62.6663	-60.9380	8	0.9988	3.5	–	<sup>10</sup> Be

**Table 5**  
Chemical composition of the bulk rock samples before chemical treatment. The data in italics correspond to the average values of the element concentrations of the samples BYC-2, BYC-4, BYC-11 (included in this study) and others of similar lithology collected in nearby areas, but not included in this study. These average values have been used for the age-exposure calculations of those samples without bulk chemical composition analysis.

Sample name	CaO (%)	K <sub>2</sub> O (%)	TiO <sub>2</sub> (%)	Fe <sub>2</sub> O <sub>3</sub> (%)	Cl (ppm)	SiO <sub>2</sub> (%)	Na <sub>2</sub> O (%)	MgO (%)	Al <sub>2</sub> O <sub>3</sub> (%)	MnO (%)	P <sub>2</sub> O <sub>5</sub> (%)	Li (ppm)	B (ppm)	Sm (ppm)	Gd (ppm)	Th (ppm)	U (ppm)
BYC-2	8.989	0.432	1.411	12.575	145	51.580	3.053	4.749	14.928	0.203	0.230	9.800	5.200	3.484	3.877	0.620	0.174
BYC-4	8.920	0.498	1.419	12.515	74	50.670	3.244	4.867	15.233	0.184	0.210	5.550	4.400	3.410	3.773	0.632	0.192
BYC-11	9.565	0.482	1.305	12.175	58	50.580	2.625	5.388	15.008	0.192	0.190	3.830	2.900	3.096	3.392	0.600	0.194
<i>Average</i>	<i>9.651</i>	<i>0.524</i>	<i>1.094</i>	<i>10.741</i>	<i>74</i>	<i>48.099</i>	<i>3.082</i>	<i>4.746</i>	<i>15.906</i>	<i>0.211</i>	<i>0.194</i>	<i>48.099</i>	<i>3.082</i>	<i>4.746</i>	<i>15.906</i>	<i>0.211</i>	<i>0.194</i>

Magnetic separation was performed on one sample (BYC-10) to isolate the abundant feldspar minerals for <sup>36</sup>Cl extraction by discarding the magnetic minerals with a magnetic separator “Frantz LB-1”. <sup>36</sup>Cl extraction from whole rock was conducted for the other 9 samples, which had insufficient amounts of feldspar minerals. In both cases, aliquots of untreated bulk sample were taken to determine the sample composition (major and trace elements; Table 5). Samples with initial weights of 120 g were rinsed and shaken with ultrapure water for 3 h to remove dust and fines. After that, between 40 and 50% of the initial weight was dissolved with a mixture of diluted nitric acid (10% HNO<sub>3</sub>) and concentrated hydrofluoric acid (48% HF) in order to remove atmospheric <sup>36</sup>Cl and potentially Cl-rich groundmass. After this partial dissolution, the remaining etched sample mass was rinsed and dried, and 2-g

aliquots were taken to determine the major element concentrations (Table 6). Compositional analyses of all aliquots were performed at the “Service d’Analyse des Roches et des Minéraux” (SARM, CRPG, Nancy, France). Before total dissolution, ~260 µL of a <sup>35</sup>Cl carrier (spike: 010813(4), 6.92 mg Cl g<sup>-1</sup>, <sup>35</sup>Cl/<sup>37</sup>Cl ratio 917.75) manufactured in-house were added to the samples for isotopic dilution (Ivy-Ochs et al., 2004), allowing for simultaneous determination of the <sup>36</sup>Cl and Cl concentrations from the <sup>36</sup>Cl/<sup>35</sup>Cl and <sup>35</sup>Cl/<sup>37</sup>Cl measurements. For the total dissolution of the rock samples, a mixture of 9 mL of 10% HNO<sub>3</sub> per gram of sample and 4.5 mL of 48% HF per gram of sample was used. After the total dissolution, the samples were centrifuged to discard the undissolved residues and gel (fluoride complexes, CaF<sub>2</sub>). Then, the chlorine in the liquid solution was precipitated to silver chloride

**Table 6**  
Concentrations of the major elements determined in splits taken after the chemical pre-treatment (acid etching). P<sub>2</sub>O<sub>5</sub> concentrations are below detection limit (0.015%).

Sample name	CaO (%)	K <sub>2</sub> O (%)	TiO <sub>2</sub> (%)	Fe <sub>2</sub> O <sub>3</sub> (%)	SiO <sub>2</sub> (%)	Al <sub>2</sub> O <sub>3</sub> (%)	MnO (%)	MgO (%)	Na <sub>2</sub> O (%)
BYC-1	8.99 ± 0.45	0.40 ± 0.10	0.78 ± 0.16	10.21 ± 0.20	55.49 ± 1.11	14.37 ± 0.29	0.19 ± 0.04	4.38 ± 0.44	8.99 ± 0.29
BYC-2	8.06 ± 0.40	0.39 ± 0.10	1.07 ± 0.11	10.71 ± 0.21	58.03 ± 1.16	13.45 ± 0.27	0.19 ± 0.04	3.86 ± 0.39	8.06 ± 0.30
BYC-3	8.15 ± 0.41	0.43 ± 0.11	1.40 ± 0.14	10.54 ± 0.21	57.13 ± 1.14	13.24 ± 0.26	0.18 ± 0.04	4.67 ± 0.47	8.15 ± 0.27
BYC-4	8.21 ± 0.41	0.49 ± 0.12	0.74 ± 0.15	9.30 ± 0.93	56.98 ± 1.14	14.41 ± 0.29	0.17 ± 0.03	4.01 ± 0.40	8.21 ± 0.33
BYC-5	8.20 ± 0.41	0.41 ± 0.04	0.87 ± 0.17	10.70 ± 0.21	57.04 ± 1.14	13.35 ± 0.27	0.20 ± 0.04	4.53 ± 0.45	8.20 ± 0.30
BYC-9	8.71 ± 0.44	0.29 ± 0.07	1.22 ± 0.12	11.03 ± 0.22	57.09 ± 1.14	11.31 ± 0.23	0.20 ± 0.04	5.75 ± 0.12	2.27 ± 0.23
BYC-10	7.51 ± 0.38	0.49 ± 0.12	1.19 ± 0.12	8.77 ± 0.88	61.48 ± 1.23	10.86 ± 0.22	0.16 ± 0.03	4.51 ± 0.45	2.00 ± 0.20
BYC-11	8.35 ± 0.42	0.35 ± 0.09	1.22 ± 0.12	10.00 ± 1.00	57.42 ± 1.15	11.45 ± 0.23	0.18 ± 0.04	5.46 ± 0.11	2.07 ± 0.21
BYC-13	8.22 ± 0.41	0.49 ± 0.12	1.04 ± 0.10	9.67 ± 0.97	57.94 ± 1.16	12.55 ± 0.25	0.18 ± 0.04	4.84 ± 0.48	2.39 ± 0.24
BYC-14	8.75 ± 0.44	0.32 ± 0.08	1.27 ± 0.13	10.70 ± 0.21	57.05 ± 1.14	11.84 ± 0.24	0.19 ± 0.04	5.58 ± 0.11	2.23 ± 0.22

(AgCl) by adding 2 ml of a silver nitrate (AgNO<sub>3</sub>) solution at 10%. To achieve this, samples were stored for 2 days in a dark place to allow the AgCl to settle down on the bottom of the bottles. This enabled the extraction of the supernatant solution (excess HF and HNO<sub>3</sub>) by a peristaltic pump avoiding the disturbance of the AgCl precipitate. In the next step, aiming to reduce the isobaric interferences of <sup>36</sup>S throughout the <sup>36</sup>Cl measurements in the Accelerator Mass Spectrometer (AMS) sulphur was removed in the form of barium sulphate (BaSO<sub>4</sub>) obtained after the re-dissolution of this first AgCl precipitate and the addition of 1 mL of a saturated solution of barium nitrate (Ba(NO<sub>3</sub>)<sub>2</sub>). BaSO<sub>4</sub> was discarded by centrifuging and filtering the supernatant with a syringe and an acrodisc filter. Then, AgCl was precipitated again with 3–4 mL of diluted HNO<sub>3</sub> (1:1 vol). The precipitate was collected after centrifuging, and was rinsed and finally dried in the oven at 80 °C for 2 days. Once the AgCl precipitate was completely dried, it was loaded in cathodes. Subsequently, targets were dried in the oven in order to protect them from atmospheric humidity until they were measured by AMS.

For the <sup>10</sup>Be extraction, the processing started with the quartz isolation from the bulk rock. Magnetic minerals were discarded by using the magnetic separator “Frantz LB-1”. After that, the non-magnetic fraction was chemically attacked at successive rounds with a mixture of concentrated hydrochloric (1/3 HCl) and hexafluorosilicic (2/3 H<sub>2</sub>SiF<sub>6</sub>) acids aiming to dissolve non-quartz minerals. Then, the remaining minerals were decontaminated from meteoric <sup>10</sup>Be by means of three successive partial dissolutions with concentrated HF, which also dissolved the remaining impurities from the previous step. The samples yielded 60–80 g of purified quartz (Table 7). Before the total dissolution, 150 µL of a <sup>9</sup>Be carrier solution (concentration: 3025 ± 9 µg g<sup>-1</sup>; Merchel et al., 2008) manufactured in-house from a phenakite crystal were added to the samples. Quartz was totally dissolved in 48% HF (3.6 mL per g of quartz + 30 mL in excess). The resulting solutions

were evaporated until dryness and samples were recovered with hydrochloric acid. Subsequently samples were precipitated with ammonia before successive separations through an anion exchange column (Dowex 1X8) to remove iron and a cation exchange column (Dowex 50WX8) to discard boron (isobar) and recover Be (Merchel and Herpers, 1999). Finally, the eluted Be was precipitated to Be(OH)<sub>2</sub> with ammonia and oxidized to BeO at 700 °C. The targets were prepared by mixing Niobium powder with the BeO oxide for AMS measurements.

The final AgCl and BeO targets were analyzed at the AMS facility ASTER “Accélérateur pour les Sciences de la Terre, Environnement et Risques” at CEREGE to measure the specific isotope ratios for <sup>36</sup>Cl (<sup>35</sup>Cl/<sup>37</sup>Cl and <sup>36</sup>Cl/<sup>35</sup>Cl) and <sup>10</sup>Be (<sup>10</sup>Be/<sup>9</sup>Be) dating. The <sup>36</sup>Cl measurements were normalized to the in-house standard SM-CL-12 with an assigned <sup>36</sup>Cl/<sup>35</sup>Cl ratio value of (1.428 ± 0.021) × 10<sup>-12</sup> (Merchel et al., 2011) and assuming a natural <sup>35</sup>Cl/<sup>37</sup>Cl ratio of 3.127. The <sup>10</sup>Be measurements were calibrated against the in-house standard STD-11, using an assigned <sup>10</sup>Be/<sup>9</sup>Be ratio of (1.191 ± 0.013) × 10<sup>-11</sup> (Braucher et al., 2015). Analytical 1σ uncertainties include uncertainties in AMS counting statistics, the standard <sup>10</sup>Be/<sup>9</sup>Be ratio, an external AMS error of 0.5% (Arnold et al., 2010) and a chemical blank measurement. A <sup>10</sup>Be half-life of (1.387 ± 0.0012) × 10<sup>6</sup> years was used (Chmeleff et al., 2010; Korschinek et al., 2010).

We calculated <sup>36</sup>Cl ages using two different procedures. On the one hand, the Excel™ spreadsheet for *in situ* <sup>36</sup>Cl exposure age calculations designed by Schimmelpfennig et al. (2009), as it allows using different <sup>36</sup>Cl production rates from spallation. In this case, the elevation-latitude scaling factors were based on the time invariant “St” scheme (Stone, 2000). The production rate of epithermal neutrons for fast neutrons in the atmosphere at the land/atmosphere interface was 696 ± 185 neutrons (g air)<sup>-1</sup> yr<sup>-1</sup> (Marrero et al., 2016). The high-energy neutron attenuation length

**Table 7**

AMS analytical data and calculated exposure ages. <sup>36</sup>Cl/<sup>35</sup>Cl, <sup>35</sup>Cl/<sup>37</sup>Cl and <sup>10</sup>Be/<sup>9</sup>Be ratios were inferred from measurements at the ASTER AMS facility. The numbers in italics correspond to the internal (analytical) uncertainty at one standard deviation. Note that the <sup>36</sup>Cl ages reported for “St” scaling were calculated through the Excel™ spreadsheet by Schimmelpfennig et al. (2009) and those for “LSD” scaling were calculated through the trial version of the CREp online calculator (Schimmelpfennig et al., 2019).

<sup>36</sup> Cl samples								
Sample name	Sample weight (g)	mass of Cl in spike (mg)	<sup>35</sup> Cl/ <sup>37</sup> Cl	<sup>36</sup> Cl/ <sup>35</sup> Cl (10 <sup>-14</sup> )	[Cl] in sample (ppm)	[ <sup>36</sup> Cl] (10 <sup>4</sup> atoms g <sup>-1</sup> )	Age (ka) “St” scaling	Age (ka) “LSD” scaling
BYC-1	78.58	1.821	13.808 ± 0.231	11.015 ± 0.702	8.8	5.54 ± 0.37	<b>11.0 ± 1.4 (1.0)</b>	<b>10.4 ± 1.2 (0.7)</b>
BYC-2	76.22	1.777	7.833 ± 0.138	8.731 ± 0.681	20.4	5.70 ± 0.47	<b>11.0 ± 1.5 (1.2)</b>	<b>10.3 ± 1.3 (1.0)</b>
BYC-3	66.44	1.809	13.201 ± 0.220	8.028 ± 0.575	10.9	4.79 ± 0.36	<b>9.7 ± 1.2 (1.0)</b>	<b>9.1 ± 1.1 (0.8)</b>
BYC-4	75.32	1.807	8.490 ± 0.142	1.207 ± 0.197	18.3	0.68 ± 0.13	<b>1.2 ± 0.3 (0.3)</b>	<b>1.1 ± 0.3 (0.2)</b>
BYC-5	75.46	1.811	10.409 ± 0.171	1.093 ± 0.176	13.4	0.53 ± 0.11	<b>1.0 ± 0.2 (0.2)</b>	<b>0.8 ± 0.2 (0.2)</b>
BYC-9	74.98	1.819	3.962 ± 0.066	1.927 ± 0.263	120.8	3.69 ± 0.59	<b>3.4 ± 0.8 (0.7)</b>	<b>3.0 ± 0.7 (0.6)</b>
BYC-10	68.10	1.814	25.547 ± 0.495	3.983 ± 0.390	4.6	1.95 ± 0.21	<b>4.4 ± 0.7 (0.6)</b>	<b>4.2 ± 0.6 (0.4)</b>
BYC-11	67.49	1.821	6.966 ± 0.121	2.753 ± 0.330	29.0	2.19 ± 0.29	<b>3.9 ± 0.7 (0.6)</b>	<b>3.6 ± 0.6 (0.5)</b>
BYC-13	70.44	1.819	19.341 ± 0.347	4.606 ± 0.422	6.3	2.32 ± 0.23	<b>5.0 ± 0.7 (0.6)</b>	<b>4.7 ± 0.6 (0.5)</b>
BYC-14	69.89	1.799	5.217 ± 0.088	2.623 ± 0.335	51.0	2.77 ± 0.39	<b>4.0 ± 0.8 (0.7)</b>	<b>3.6 ± 0.7 (0.6)</b>
<sup>36</sup> Cl Blanks					Total atoms Cl (10 <sup>17</sup> )	Total atoms <sup>36</sup> Cl (10 <sup>4</sup> )		
BL-1	–	1.805	353.174 ± 11.131	0.265 ± 0.073	2.252 ± 0.160	8.264 ± 2.264	–	–
BL-5	–	1.822	362.525 ± 8.014	0.290 ± 0.075	2.177 ± 0.133	9.133 ± 2.377	–	–
<sup>10</sup> Be samples								
Sample name	Quartz weight (g)	mass of carrier ( <sup>9</sup> Be mg)	<sup>10</sup> Be/ <sup>9</sup> Be (10 <sup>-14</sup> )	[ <sup>10</sup> Be] (10 <sup>4</sup> atoms g <sup>-1</sup> )	Age (ka)			
BYC-12	64.5799	152.29	5.644 ± 0.286	2.701 ± 0.137	<b>5.5 ± 0.4 (0.3)</b>			
BYB-10	82.2924	151.98	4.719 ± 0.496	1.762 ± 0.185	<b>3.5 ± 0.4 (0.4)</b>			
<sup>10</sup> Be Blank								
BYB-BK	–	151.29	–	–	–	–	–	–

value applied was  $160 \text{ g cm}^{-2}$ . We used the following  $^{36}\text{Cl}$  production rates –references to sea-level and high latitude (SLHL)– from spallation of different elements:  $42.2 \pm 4.8 \text{ atoms } ^{36}\text{Cl} (\text{g Ca})^{-1} \text{ yr}^{-1}$  for Ca spallation (Schimmelpfennig et al., 2011),  $148.1 \pm 7.8 \text{ atoms } ^{36}\text{Cl} (\text{g K})^{-1} \text{ yr}^{-1}$  for K spallation (Schimmelpfennig et al., 2014),  $13 \pm 3 \text{ atoms } ^{36}\text{Cl} (\text{g Ti})^{-1} \text{ yr}^{-1}$  for Ti spallation (Fink et al., 2000),  $1.9 \pm 0.2 \text{ atoms } ^{36}\text{Cl} (\text{g Fe})^{-1} \text{ yr}^{-1}$  for Fe spallation (Stone et al., 2005). On the other hand, we calculated the  $^{36}\text{Cl}$  exposure ages using the trial version of the online calculator CREp for  $^{36}\text{Cl}$  (Schimmelpfennig et al., 2019), where the “LSD” (Lifton–Sato–Dunai) elevation latitude scaling scheme was implemented, together with the LSD geomagnetic database framework (Lifton et al., 2014) and the same production rates from the spallation of the abovementioned elements. As Ca spallation is the most dominant  $^{36}\text{Cl}$  production reaction and the Schimmelpfennig et al. (2011) production rate was calibrated at the Etna volcano (i.e. an area with a different atmospheric setting from the Antarctica sampling sites), we corrected the atmospheric pressure of the sampling sites. South Shetland Islands are affected by permanent subpolar low-pressure systems, which affect the cosmic-ray particle flux so that it influences (i.e. increases) the local cosmogenic nuclide production rate. Consequently, this atmospheric pressure anomaly has to be taken into account when scaling the SLHL production rates. In fact, Dunai (2010) advises including any long-term atmospheric pressure anomaly at least for Holocene exposure periods. Thus, the atmospheric pressure value was corrected for the elevation of each sampling site by implementing the ERA40 (Uppala et al., 2005) atmosphere model using the MATLAB function “ERA40.mat” (Lifton et al., 2014). The specific Antarctica

atmosphere model (Stone, 2000) was not used as the atmosphere in continental Antarctic is affected by the air flow over the ice-sheet, which impacts the elevation/air pressure relationship in the opposite way (thermal high pressure at surface level). The  $^{36}\text{Cl}$  ages that will be presented and discussed throughout this work are those obtained from the “LSD” scaling scheme so that they are comparable to the  $^{10}\text{Be}$  ages.

Finally,  $^{10}\text{Be}$  exposure ages were calculated by using the online calculator “CREp” (Martin et al., 2017; available online at: <http://crep.crgp.cnrs-nancy.fr/#/>). In this calculator, we applied again the “LSD” elevation latitude scaling scheme (Lifton et al., 2014), the ERA40 atmospheric model (Uppala et al., 2005) and the geomagnetic database based on the LSD framework (Lifton et al., 2014). These parameters yield a SLHL  $^{10}\text{Be}$  production rate from Be spallation of  $3.98 \pm 0.22 \text{ atoms g}^{-1} \text{ yr}^{-1}$ .

We include the results, with total error and analytical errors in Table 7 and Fig. 3. In the text and in the figures we show the results with the total error. We do not have any quantitative information on the snow cover during the surface exposure duration. Therefore, samples were taken from surfaces that are exposed to strong winds, in order to limit the potential effects of prolonged snow cover on the cosmogenic nuclide production. We also avoided surfaces that showed signs of significant erosion or spalling. In addition, denudation rates in Antarctica are reported to be extremely low (0–1 m/Ma; e.g. Schäfer et al., 1999; Balco et al., 2014), thus having no significant effect on the Holocene exposure ages. Hence, no corrections for potential effects of snow cover or denudation were applied to the ages, in consistency with other studies from this region (e.g. Ciner et al., 2019).

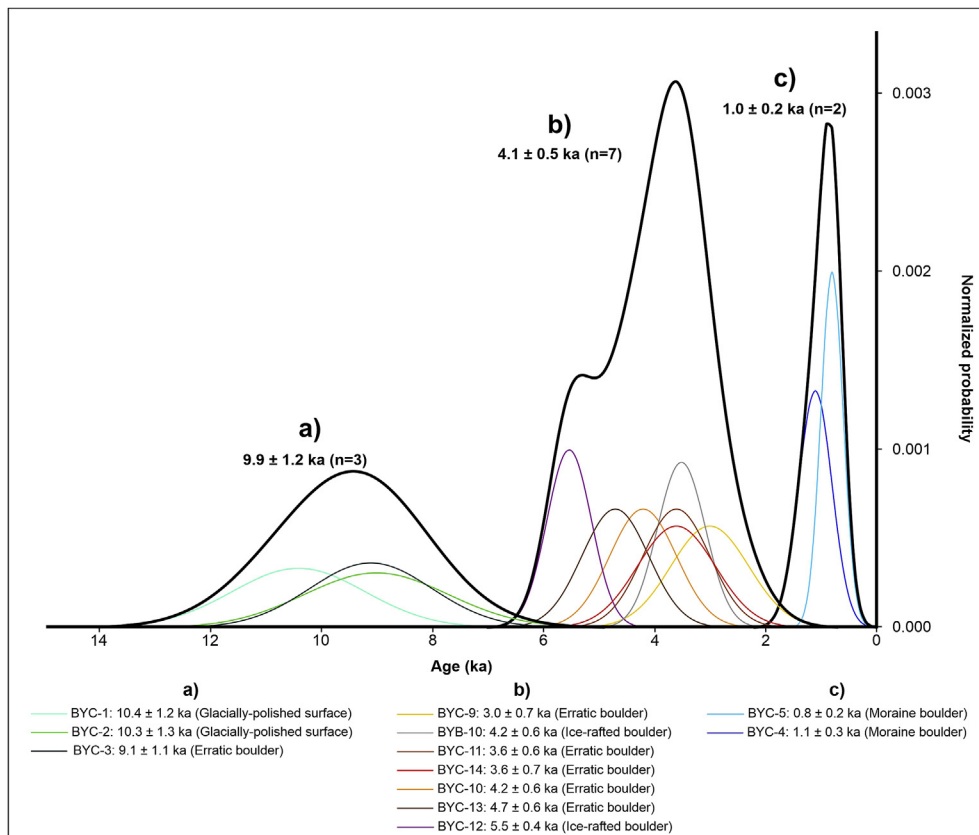
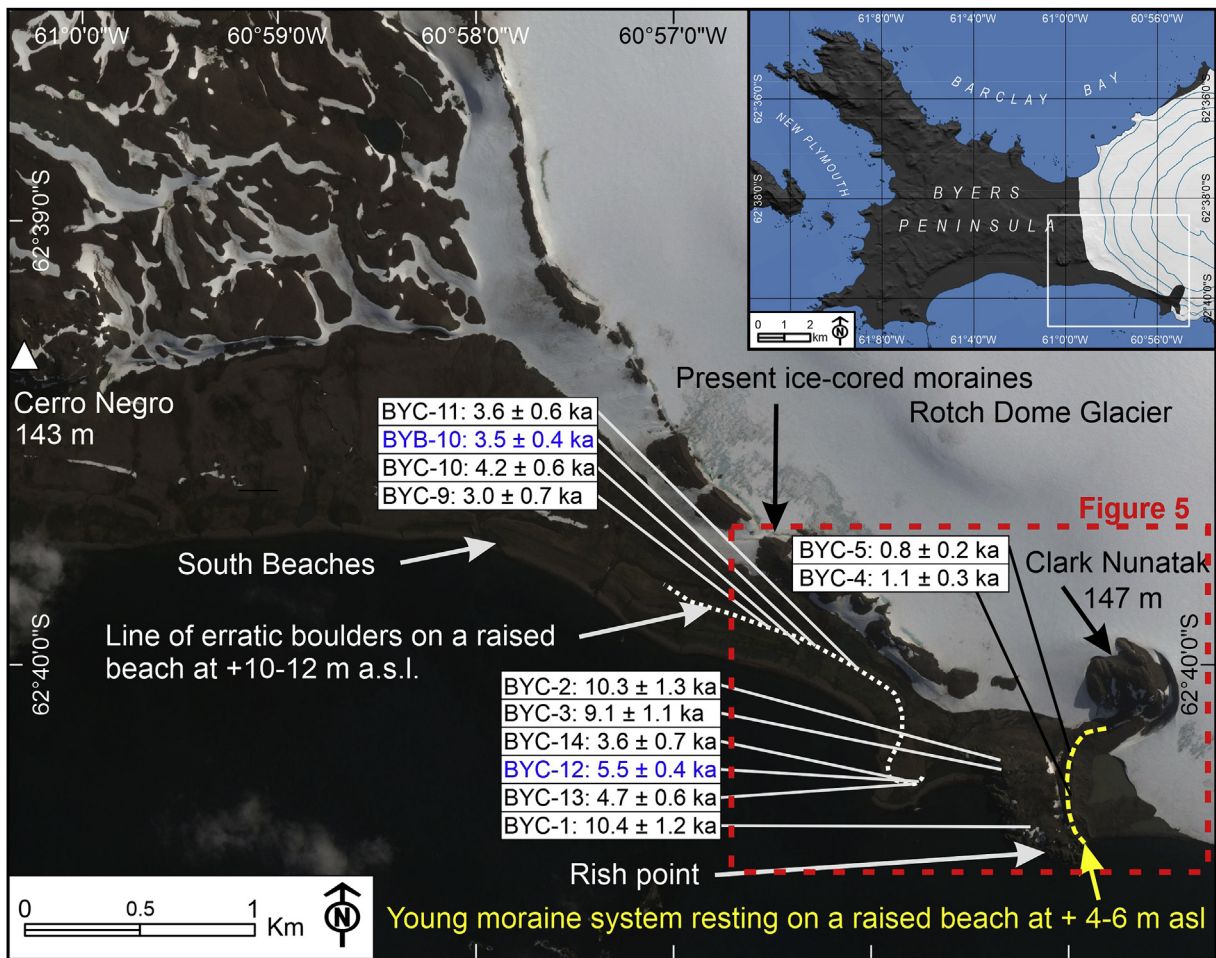


Fig. 3. Probability density plots of CRE ages for differentiated chronostratigraphical units: A) Deglaciation, b) First Neoglacial advance and c) Second Neoglacial advance. This figure is available in colour in the online version.



**Fig. 4.** Location of the study area, with the main geomorphological features, CRE samples and their ages plotted in a Google Earth satellite image. This figure is available in colour in the online version.

## 5. Results of the timing of neoglacial advance in the Byers Peninsula

### 5.1. Geomorphological setting of neoglacial landforms

The ice-cored moraine system in the present front of the Roch Dome Glacier is formed by sharp-crested ridges standing 50–70 m above the adjacent bedrock surface, with blocks >1 m in diameter (Figs. 4–6). The extensive debris cover has a very high ice proportion, exceeding 60% of the total volume, according to field observations. The sediments are distributed in the direction of the glacier's foliation and its lithology reflects that of the basalt bedrock, which indicates that the moraine results from basal and englacial debris. From the moraine crests, a steep ramp of ice (40° slope) descends to the southern side of the peninsula. The unconsolidated sediments of the moraines are currently being intensely reworked by mass wasting processes, and are thus not appropriate for surface exposure dating methods (lichenometry or CRE).

This ice-cored moraine ridge overrides all raised beaches from the central plateau to the 6 m a.s.l. raised beach in the N and S coastal fringes (Fig. 4). Our research focuses on the southern sector of the moraine system, where it overlaps the raised beaches until the Clark Nunatak. Just SW of this nunatak, a small peninsula – called Rish Point – formed by a series of volcanic plugs stands only at 60 m from the coast line (Figs. 4–6).

Next to the highest volcanic plug of the area (Ritli Hill, 45 m)

(Figs. 4–7), we observed a glacial polished surface at an elevation of 28 m, and a distance of 600 m southwards of the present moraine ridge. Here, we collected the bedrock sample BYC-1. On another volcanic plug, only 350 m from the moraine ridge and at elevation of 47 m, another polished surface was observed with an erratic on it. Samples were taken from bedrock surface BYC-2 and from the erratic boulder BYC-3.

On the western side of the Clark Nunatak, the ice ramp descending from the external part of the ice-core moraine ridge does not connect with the bedrock surface but to thick layers of till, which rest on the 10–12 m a.s.l. raised beach. At the connection between the till deposits and the raised beach, there is a group of large, stable erratic glacial boulders, aligned parallel to the limit of the glacier. This line of erratic boulders is located about 200 m to the S of the present glacier front and lies on the 10–12 m a.s.l. beach. These boulders are basalts and we assume that were deposited by Dome Rotch glacier during a small advance, when it trespassed the 10–12 m a.s.l. beach. The five largest and most stable basaltic boulders were selected from this line to take samples for  $^{36}\text{Cl}$  dating (BYC-9, 10, 11, 13 and 14) (Figs. 5, 6 and 8). In addition to the erratic basaltic boulders that rest on the 10–12 m a.s.l. raised beach, there are some granite boulders that were embedded in the sediments of this raised beach protruding around a meter above the beach sand level. We assume that these granitic boulders were transported by icebergs from the AP during the beach formation, as there are no granitic rocks in Byers bedrock (Hall and Perry, 2004).

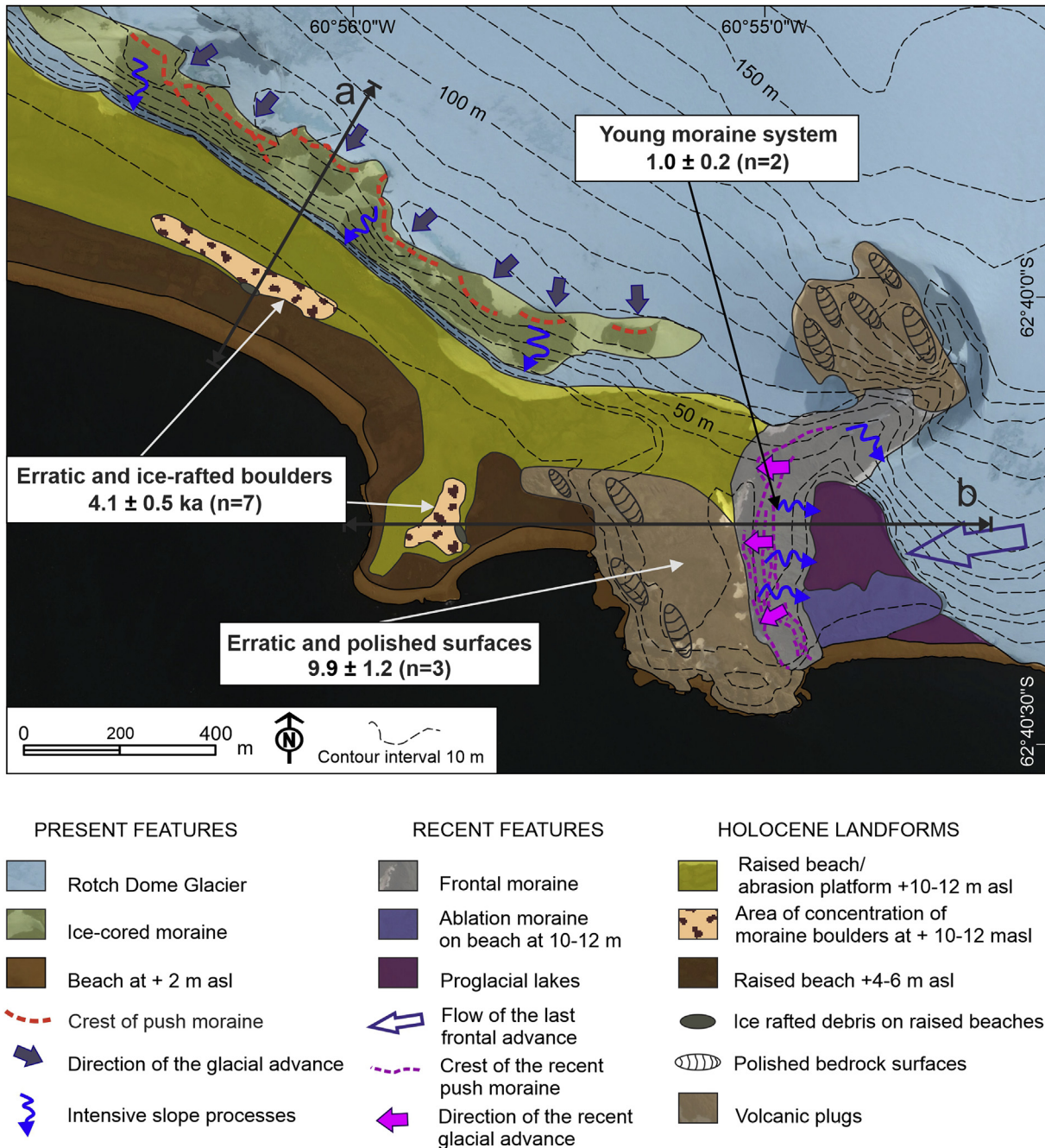


Fig. 5. Geomorphological sketch with CRE arithmetic mean ages for each geomorphological unit. This figure is available in colour in the online version.

We sampled two of the ice rafted granitic boulders (BYB-10 and BYC-12) (Figs. 4–6 and 8 and 9). We assume that the ice-rafted boulders have been stable since they were deposited on the beach, and therefore CRE ages of these boulders must coincide with the age of formation of the beach where they are distributed.

On the other hand, there is a moraine ridge surrounding the W side of Clark Nunatak and with the eastern extreme of Rish Point, which trespassed the 4–6 m a.s.l. raised beach. This is one of the few sites in the Byers Peninsula where the current front of the glacier is separated from the ice-core moraine crest (distance of ca. 500 m). This moraine is formed by several crests and arcs that overlap one another. The youngest arcs constitute ice-cored moraine ridges and are very unstable and subject to mass

movements and intense remobilization. The outer most crests are stable. Two boulders from this stable older sector of the moraine were selected for CRE samples (BYC-4 and 5), located at elevation of 35 m (Figs. 4–6 and 10).

### 5.2. CRE results

CRE results show a complex spatio-temporal pattern with regards to the glacial evolution during the Mid-Late Holocene in the Byers Peninsula.

The oldest ages correspond to the deglaciation of the Rish Point. Samples BYC-1 and 2 on the two polished surfaces located on the summit of volcanic plugs reported the same <sup>36</sup>Cl age of 10.4 ± 1.2

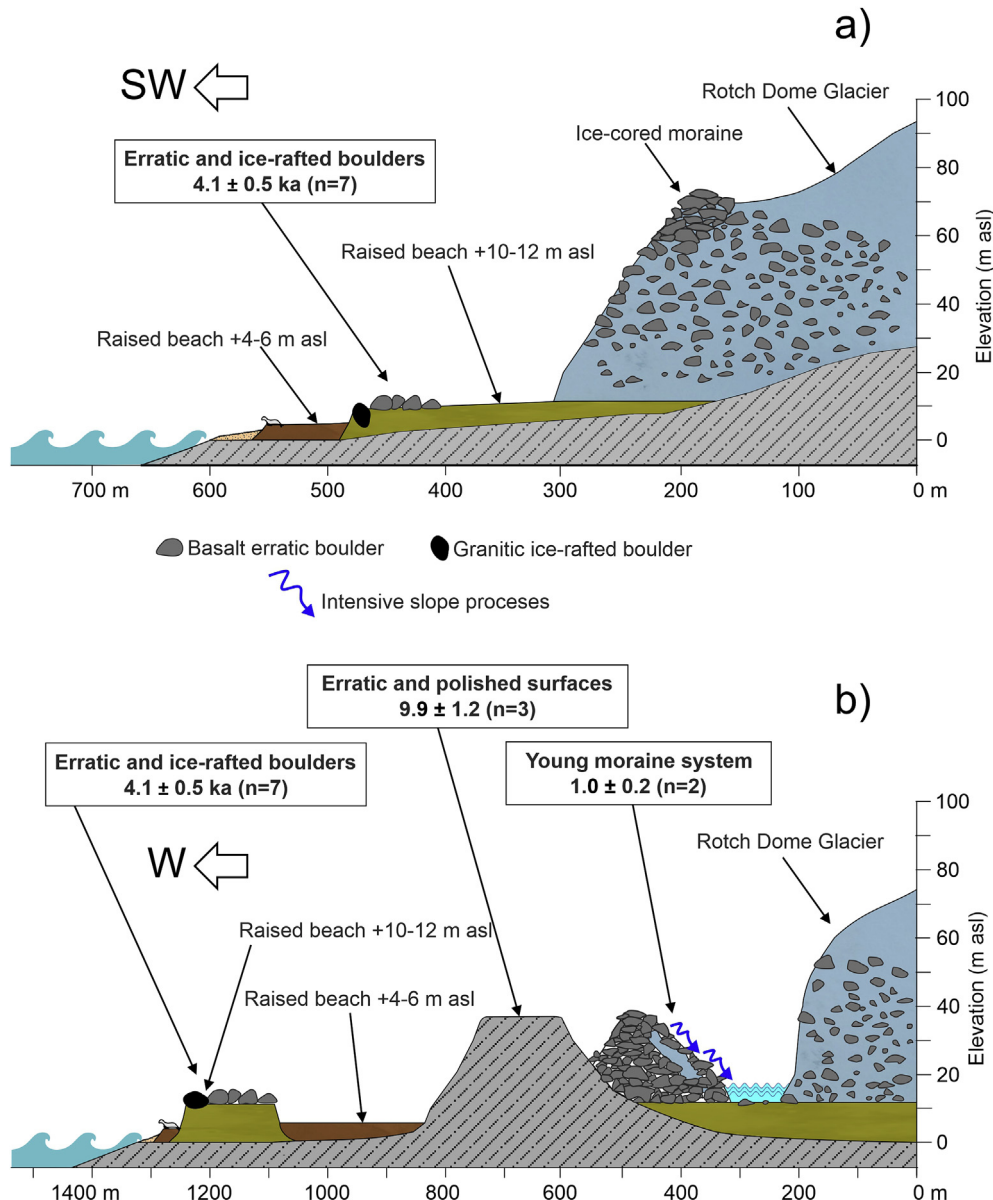


Fig. 6. Geomorphological transect of the main features with arithmetic mean of the CRE ages in each unit. This figure is available in colour in the online version.

and  $10.3 \pm 1.3$  ka. The erratic boulder BYC-3 deposited on the same polished surface as BYC-2 yielded a slightly younger  $^{36}\text{Cl}$  age of  $9.1 \pm 1.1$  ka. The arithmetic mean of these three samples is  $9.9 \pm 1.2$  ka ( $n = 3$ ) (Figs. 3–6 and Table 7).

The samples taken from the erratic boulders lying on the 10–12 m a.s.l. raised beach (BYC-9, 10, 11, 13 and 14) yielded the following  $^{36}\text{Cl}$  ages:  $3.0 \pm 0.7$ ,  $4.2 \pm 0.6$ ,  $3.6 \pm 0.6$ ,  $4.7 \pm 0.6$  and  $3.6 \pm 0.7$  ka, respectively. The arithmetic mean is  $3.8 \pm 0.6$  ka ( $n = 5$ ). The ages of the granitic boulders embedded in the 10–12 m a.s.l. raised beach (BYB-10) and on the littoral platform (BYC-12) give  $^{10}\text{Be}$  ages of  $3.5 \pm 0.4$  ka and  $5.5 \pm 0.4$  ka, respectively, with an arithmetic mean of  $4.4 \pm 0.4$  ka ( $n = 2$ ). In fact all these ages are indistinguishable from each other with an average of  $4.1 \pm 0.5$  ka ( $n = 7$ ) (Figs. 3–6 and Table 7).

The two boulders distributed on the moraine from the eastern flank of the Clark Nunatak where the front of the glacier has significantly retreated over the last decades (BYC-4 and 5) showed similar  $\text{Cl}^{36}$  ages of  $1.1 \pm 0.3$  and  $0.8 \pm 0.2$  ka, respectively. The mean

is  $1.0 \pm 0.2$  ka ( $n = 2$ ) (Figs. 3–6 and Table 7).

## 6. Discussion

### 6.1. Analysis of the results in the context of the SSI and the AP

The here presented first CRE dates from the Byers Peninsula indicate the existence of three different periods concerning glacier evolution in the area. The first group of landforms correspond to the polished surfaces and the erratic boulder located in Rish Point. These samples are indicative of the northwards retreat of Rotch Dome Glacier, which occurred at around 11–9 ka ( $9.9 \pm 1.2$  ka;  $n = 3$ ). This ice-free corner was deglaciated prior to the oldest raised beaches distributed at 15–16 m a.s.l. that were dated at 7.4 cal ka BP in the Byers Peninsula (Hall, 2003, 2010). The age of these landforms fits also with the chronological framework of deglaciation inferred from lake records in this peninsula, suggesting that the initial deglaciation of the central plateau took place at

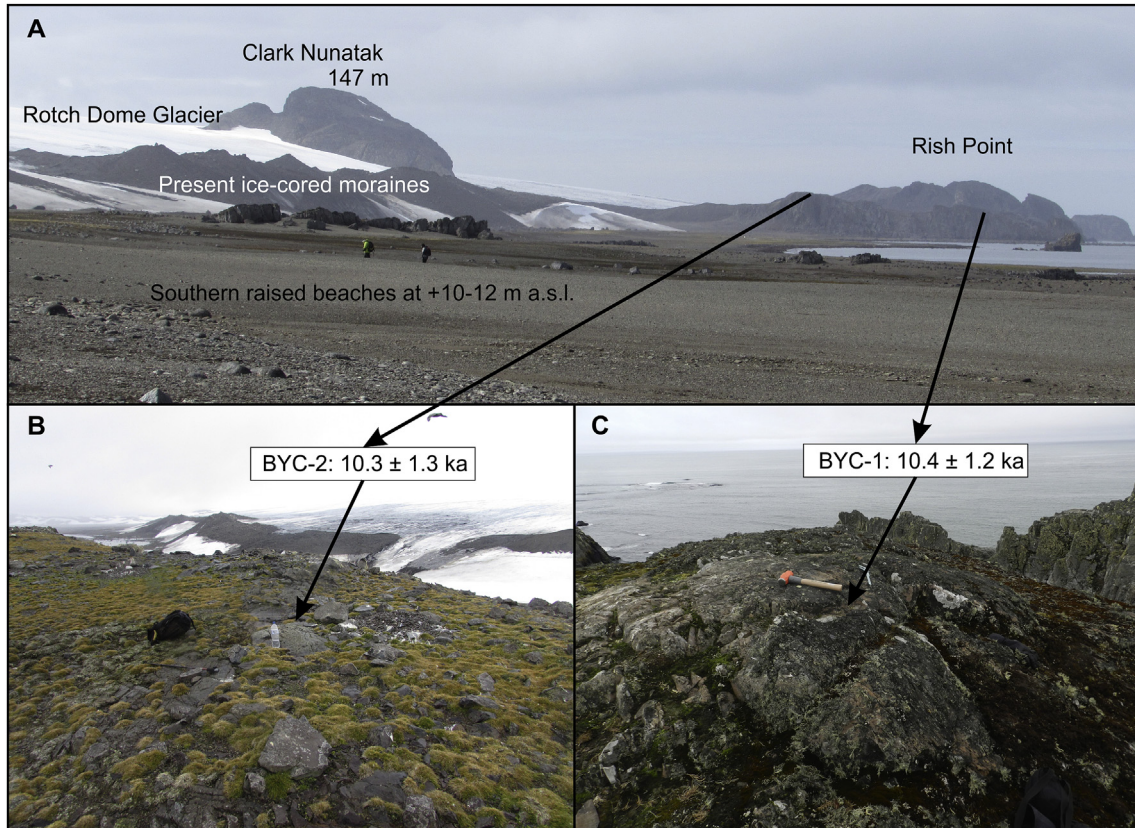


Fig. 7. BYC-1 and -2 samples and CRE ages in Rish Point, Byers Peninsula. This figure is available in colour in the online version.

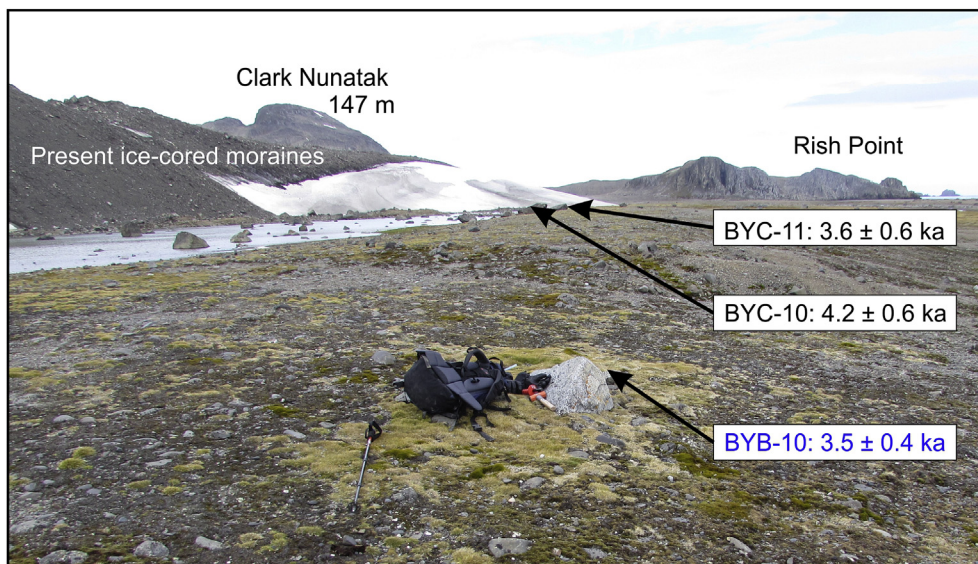
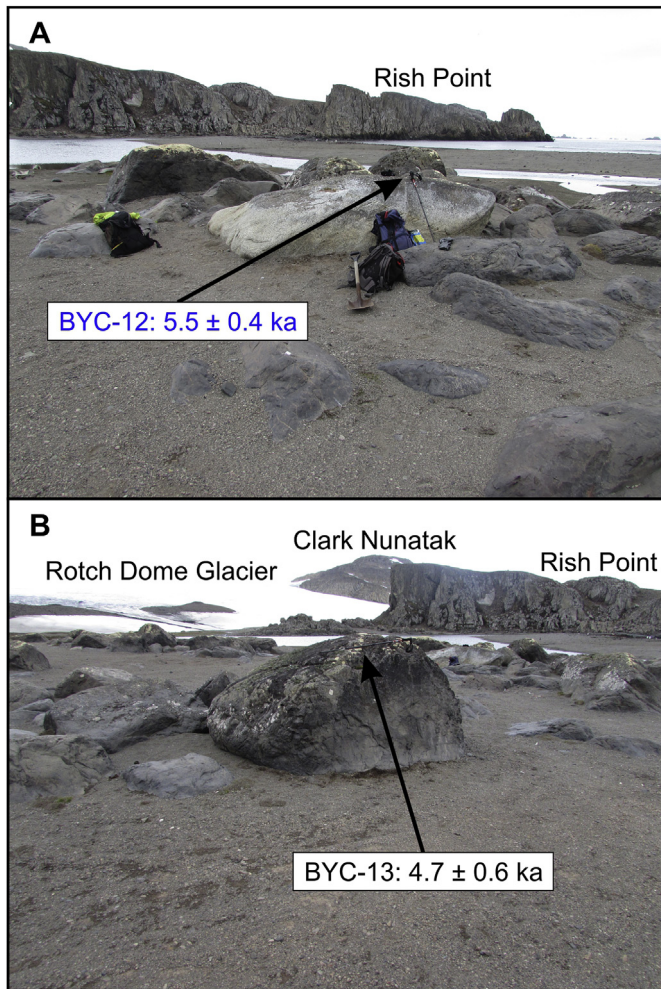


Fig. 8. BYC-11 and -12 and BYB-10 samples and CRE ages on South Beaches area, Byers Peninsula. This figure is available in colour in the online version.

8.3 cal ka BP (Toro et al., 2013; Oliva et al., 2016). The Early Holocene deglaciation of coastal environments also occurred between 9 and 6 ka in the rest of the SSI (Barsch and Mäusbacher, 1986; Mäusbacher, 1991; Del Valle et al., 2002; Hall, 2003, 2010; Bentley et al., 2005; Watcham et al., 2011), or even before 9 ka (Milliken et al., 2009; Seong et al., 2009; Simms et al., 2011a, b). This timing also coincides with data from other records from the AP,

such as marine sediments, which show a clear warming trend beginning 12 ka ago (Shevenell et al., 2011), as well as from CRE dating of glacial landforms in this peninsula (White et al., 2011; Glasser et al., 2014; Anderson et al., 2017) (Fig. 11).

A second group of landforms includes glacial basaltic boulders distributed on the beach and littoral platform at 10–12 m a.s.l (BYC 9, 10, 11, 13 and 14) and the two ice rafted granitic boulders



**Fig. 9.** BYC-12 and -13 samples and CRE ages in front of Rish Point, Byers Peninsula. This figure is available in colour in the online version.

embedded in the sediments of this raised beach (BYB 10) or located on the same littoral platform (BYC 12). The results obtained show very similar ages for all types of boulders, both basalts and granites, with an average of  $4.1 \pm 0.5$  ka ( $n = 7$ ). Therefore, the ages of the stabilization of these boulders transported by the Rotch Dome Glacier should correspond to the age of this beach level, where ice rafted granitic boulders are embedded. Radiocarbon dating from whale bones of similar altitude raised beach in the South Beaches, suggested younger ages, between 2.6 and 2 cal ka BP (Hansom, 1979; Hall and Perry, 2004; Hall, 2003, 2010). These data coincide with OSL dates of this level of raised beaches from other islands in this archipelago, between 2.3 and 2.1 ka (Simms et al., 2011a, 2012). Our results from the ice-drafted granitic boulders indicated older ages for this raised beach,  $4.4 \pm 0.4$  ka ( $n = 2$ ), which are synchronous with the glacial boulders that are distributed on it. There is a lack of correspondence between the older ages of the erratic and ice-rafted boulders and the former much younger radiocarbon dates attributed to this raised beach. To understand this apparent contradiction, it is important to highlight that there is no direct dating of the raised beach in the area. Landforms at similar altitudes within the same region do not necessarily have identical chronologies, as glacio-isostatic uplift rates enhanced also by neotectonic activity vary throughout the archipelago (Bentley et al., 2005; Fretwell et al., 2010; Simms et al., 2018). In fact, it seems reasonable that the raised beach at +10–12 m a.s.l. where the erratic boulders

are distributed may constitute an intermediate level between the raised beach dated at 2.6 and 2 cal ka BP in other sectors of the SSI and the highest raised beach of +15–17 m a.s.l., which was dated at 7.4 cal ka BP in different areas of this archipelago (Fig. 11).

The ages of glacial boulders prove the existence of a neogacial advance in the Byers Peninsula occurred ~4 ka. Until now, no such advance had been proposed, although Hall and Perry (2004) related the 10 m raised beach to a cold period with abundant rich ice-rafted debris, and Everett (1971) proposed the same for the 10–12 m a.s.l. raised beach existing in the Hurd Peninsula. Previous studies proposed that the glacier fronts in the Byers Peninsula, as well as in the rest of the SSI, were approximately at their present-day position by 5.5 ka (Barsch and Mäusbacher, 1986; Mäusbacher et al., 1989; Björck et al., 1991, 1993; 1996b; Mäusbacher, 1991; Del Valle et al., 2002; Hall, 2003, 2010; Bentley et al., 2005; Watcham et al., 2011; Simms et al., 2011a, 2012; Toro et al., 2013; Oliva et al., 2016). Our results highlight the occurrence of a limited neogacial advance at ~4 ka not exceeding 200 m from the present-day glacier front. Consequently, due to the small extent of this neogacial expansion, it may have not been detected yet in other areas. There is evidence of a cold period in the SSI before 4 ka according to the analysis of lake (Björck et al., 1991) and marine sediments (Milliken et al., 2009; Chu et al., 2017). In the context of the entire AP area and the rest of the continent, as discussed above, there is robust paleoenvironmental evidence that colder conditions with neogacial associated advances occurred around 5 ka and were interrupted by the thermal maximum around 4–3 ka (Zale and Karlén, 1989; Mosley-Thompson, 1996; Ingólfsson et al., 1998, 2003; Khim et al., 2002; Strelin et al., 2006; Heroy et al., 2008; Bentley et al., 2009; Hall, 2009; Michalchuk et al., 2009; Davies et al., 2012, 2017; Shevenell et al., 2011; Carrivick et al., 2012; Cofaigh et al., 2014; Barnard et al., 2014; Kaplan et al., 2020) (Fig. 11).

The last set of glacial landforms corresponds to the moraine ridges of the Rotch Dome Glacier on the southern flank of Clark Nunatak. This is the only area where the glacier is now spatially disconnected from the moraine and includes evidence of a Late Holocene advance of the glacier around the nunatak. Till and disperse erratic boulders are distributed on the 4–6 m a.s.l. raised beach. The BYC-4 and 5 samples were taken from the highest and most stable sector of the moraine showing an average age of ~1 ka. Although, to date, a similar advance has not been confirmed during this time in the SSI, there is some sedimentological evidence pointing to that fact. Barsch and Mäusbacher (1986) suggested two neogacial advances at 3 and 1 cal ka BP in the SSI. Björck et al. (1991) proposed a cold period in the Byers Peninsula between 1.5 and 0.5 cal ka BP. Hall and Perry (2004) delimited two cold periods at 0.25 and 1.7 cal ka BP. Hall (2009) used the CRE  $^{10}\text{Be}$  methodology to date moraines in the Hurd Peninsula and Marion Cove to 1.5–1.0 ka (Hall and Stone, personal communications). Simms et al. (2011a) indicated a neogacial advance that ended at approximately 1.7 cal ka BP in Maxwell Bay (King George Island). Lake Domo, which is very close to the study area and located only 350 m from the present-day glacier front, was deglaciated around 1.8 cal ka BP, probably after a neogacial advance (Oliva et al., 2016). Chu et al. (2017) proposed the onset of neogacial advances in the Fildes Peninsula at 2.7 cal ka BP. As discussed before, plentiful evidence from the AP confirm the occurrence of glacial advances between 2.8 and 1.4 ka (Mosley-Thompson, 1996; Björck et al., 1996a, b; Khim et al., 2002; Heroy et al., 2008; Bentley et al., 2009; Yoon et al., 2010; Domack et al., 2001; Strelin et al., 2006; Michalchuk et al., 2009; Allen et al., 2010; Davies et al., 2012, 2014; Mulvaney et al., 2012; Shevenell et al., 2011; Mulvaney et al., 2012, 2012; Abram et al., 2013; Hodgson et al., 2013; Barnard et al., 2014; Čejka et al., 2019; Kaplan et al., 2020) (Fig. 11).

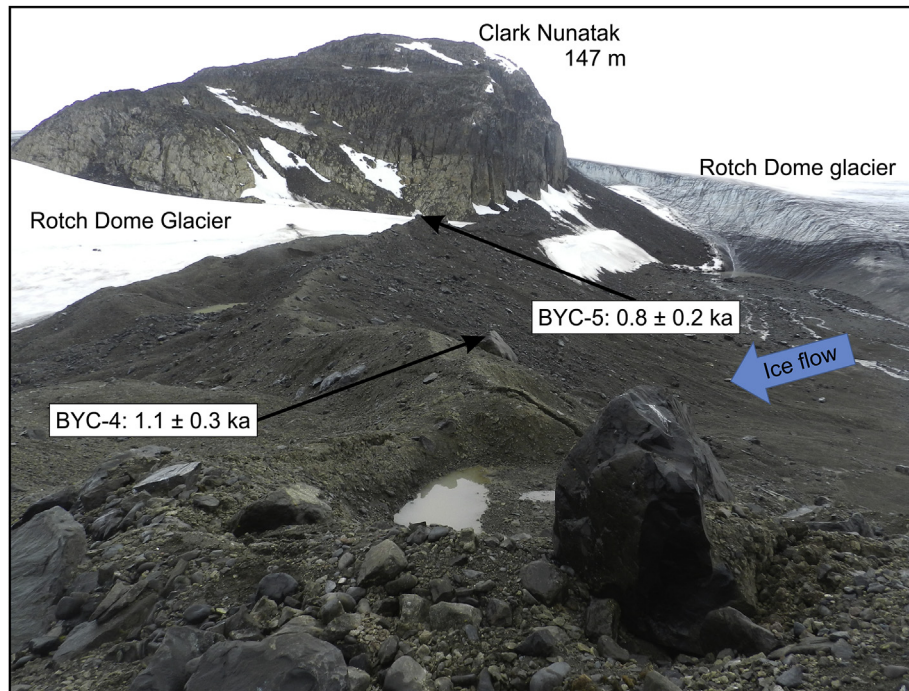


**Fig. 10.** BYC-4 and -5 samples and CRE ages in the moraine between Rish Point and Clark Nunatak, Byers Peninsula. This figure is available in colour in the online version.

As in previous glacial landforms, the ages of the moraine boulder (~1.0 ka) contradict the age of the raised beach where they rest (LIA). In fact, this raised beach at about 6 m a.s.l. has been dated in the Byers Peninsula and other islands as belonging to the LIA, between approximately the 13 and 17th centuries AD (Everett, 1971; John and Sugden, 1971; John, 1972; Sugden and John, 1973; Curl, 1980; Sugden and Clapperton, 1986; Clapperton and Sugden, 1988; Hall, 2007; Hall, 2010; Simms et al., 2011a, 2012) (Fig. 11).

The only place where a moraine similar to the one studied in this work has been directly dated in the SSI was the Collins Glacier moraine in the Fildes Peninsula by Hall (2007), according to radiocarbon ages of mosses incorporated into the interior of the moraine. As in our study area, this sector of moraine was almost the only area where the moraine was separated from the present Collins Glacier front, and was also at a distance of about 500 m. The first results of this work indicated that the most external advance was 2.8 to 1 cal ka BP, although Hall (2007) discards this possibility, precisely because the moraine rests on the 6 m a.s.l. beach.

The discordance between the ages of the moraines dated by CRE ages and the ages of raised beaches provided by radiocarbon dating of organic fragments present in their sands will remain a topic of debate until we directly date the studied raised beaches instead of basing their age on a simple correlation of altitudes. This approach could lead to important errors related to the regional variability and local neo-tectonics (Bentley et al., 2005; Fretwell et al., 2010; Simms et al., 2018).

The results suggest that these younger moraines may be somewhat older than the LIA, as previously thought (Everett, 1971; John and Sugden, 1971; John, 1972; Sugden and John, 1973; Curl, 1980; Sugden and Clapperton, 1986; Clapperton, and Sugden, 1988; Hall, 2007, 2010). Our proposal is that they are polygenic moraines formed by several neoglacial advances driven by cold periods that may have expanded from 2 ka to the LIA, as has been proposed in many other areas of the AP (Zale and Karlén, 1989; Domack et al., 2001; Hall and Denton, 2002; Allen et al., 2010; Storey et al., 2010; Michalchuk et al., 2009; Balco and Schaefer,

2013; Davies et al., 2014, 2017). In fact, although the outermost crest of the moraine dates back to ~1.0 ka, based on our results (Fig. 4), the glacier must have retreated from the moraine limits very recently, probably after 1950, as occurred in the nearby peninsula of Elephant Point (Oliva and Ruiz-Fernández, 2015, 2017) (Fig. 11).

The available proxy data for the Mid and Late Holocene does not yet allow to constrain which climate parameters are responsible for such glacial oscillations. Bentley et al. (2009) provided evidence of the occurrence of relative warmth from 4.5 to 2 cal ka BP in the AP region, which is also confirmed by ice core records from the NE corner of the AP reporting relative stable temperature until 2.5 ka BP when climate cooled (Mulvaney et al., 2012). Past surface air temperature changes are similar to those inferred from several sites across the AP from moss banks (Charman et al., 2018).

## 6.2. The Neoglaciation of the SSI and the AP in a global context

Despite significant regional variations in the timing of Neoglaciation in the AP, there are some common patterns in all records: the end of maximum deglaciation occurred at around 7–6 ka and the first neoglacial started at 5 ka, with new and previously undated neoglacial advances between 2.7 and 1 ka, and even up to the LIA, before the RRW. Most records in the SSI are not concurrent with neoglacial timing in the AP. This can be related to the different nature of the records and dating methods used in each study. In fact, each of the proxies examined in this work (ice core, marine and lake sediments, raised beaches and glacial landforms) as well as the dating methods have been substantially refined over the last years and inter-comparisons between areas and methods are needed to homogenize and compare results (e.g. Simonsen et al., 2019; Singer et al., 2019; Sadatzki et al., 2019; Čejka et al., 2019). However, our data show that the chronology inferred directly from glacial landforms shows a similar timing for neoglacial advances in the SSI and the AP. Recently, Kaplan et al. (2020) highlighted synchronous millennial-scale neoglacial oscillations in the NE edge of

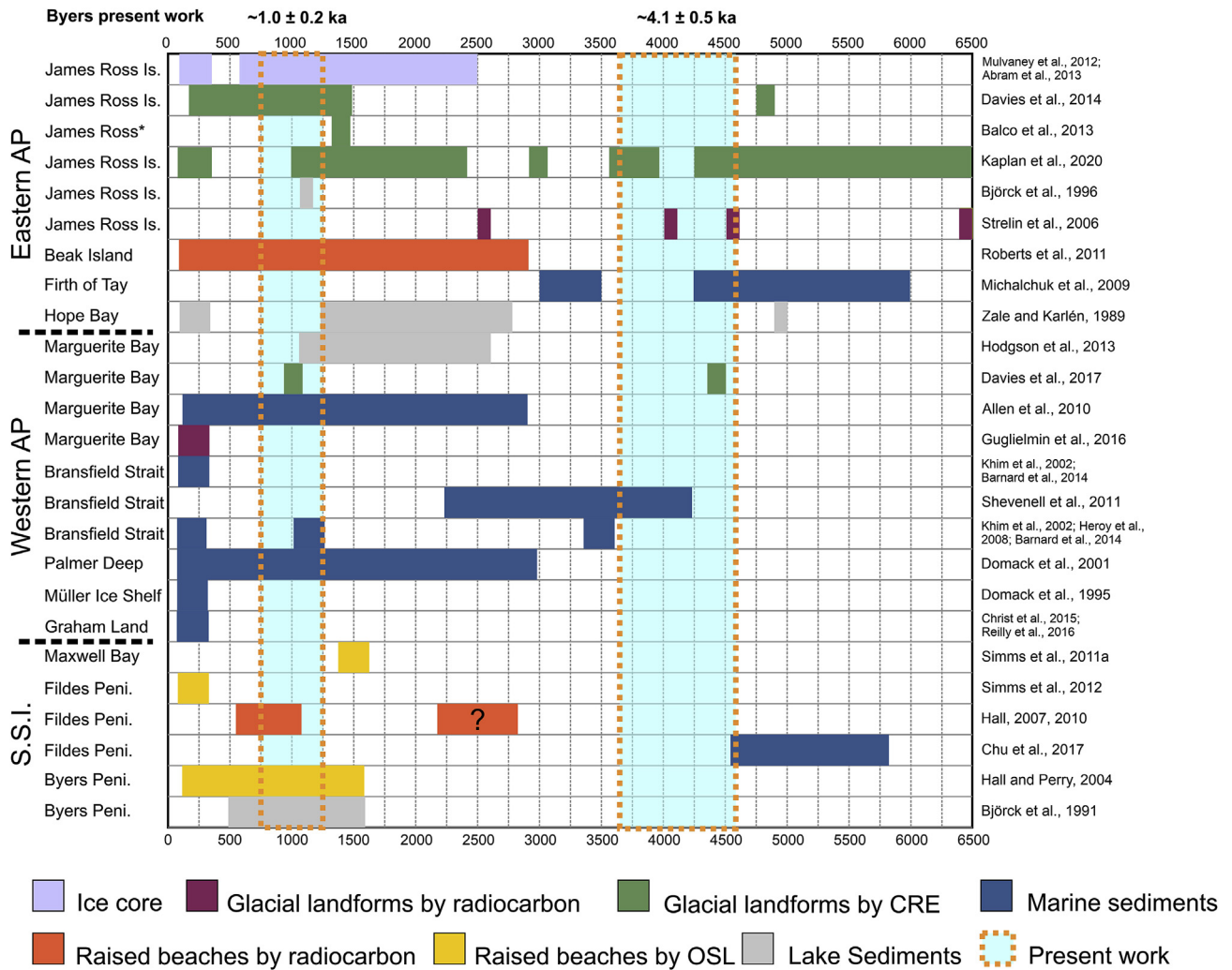


Fig. 11. Summary table comparing the timing of neoglacial expansion in the AP region and the results of this work. This figure is available in colour in the online version.

the AP and in Patagonia. These authors proposed that these neoglacial advances coincided with negative phases of the Southern Annular Mode (SAM), when the westerly winds expanded towards the equator. In line with this, the current RRW coincides with a positive phase of the SAM that is favoring widespread glacial retreat in both regions (Abram et al., 2014).

The comparison of Neoglaciation in the AP with the Arctic records may reveal whether neoglacial advances follow interhemispheric connection between polar regions. However, neoglacial advances within the Arctic show a very different pattern, even more divergent than within the AP (Solomina et al., 2015; McKay et al., 2018). Throughout the Arctic, the end of deglaciation varied from 11 to 5 ka depending on the region (Renssen et al., 2012). The first phases of neoglacial advances were detected between 9 and 7 ka in Scandinavia and 4 ka in Greenland (Solomina et al., 2015; McKay et al., 2018). In any case, there are also some common patterns for the entire Arctic, which are quite similar to those observed in the AP. According to the most recent synthesis, glaciers retreated throughout the Arctic from 8.6 to 5 ka (Marcott et al., 2013; Solomina et al., 2015; Kaufman et al., 2016; Sejrup et al., 2016; Briner et al., 2016; McKay et al., 2018; Geirsdóttir et al., 2019), similarly to what happened in the SSI and the AP. After this widespread retreat, there are two main phases of generalized neoglacial expansion in (almost) all regions across the Arctic, one beginning at

4.5 ka and another from 2 ka to the LIA (Solomina et al., 2015; Miller et al., 2013; Miller et al., 2017; McKay et al., 2018; Geirsdóttir et al., 2019). A similar timing for glacial advances was also identified in the SSI and the AP.

Therefore, there is a common global pattern at a millennia timescale with regards to the Neoglaciation dynamics in glaciers of the AP and in the Arctic. These patterns are similar to those found in the Byers Peninsula: intensive deglaciation around 8.6 to 5 ka, followed by the first neoglacial advances around 4.5 ka and new, intensive neoglacial advances around 2 ka. This Late Holocene glacier behavior in the high latitudes of both hemispheres is very different from the evolution of temperatures that occurred in the two regions during Termination I, when temperature changes were simultaneous but inverse in the two hemispheres, the pattern known as “bipolar seesaw” (Broecker and Denton, 1990; Barker et al., 2009, 2010). The opposite temperature trends recorded in Antarctica and Greenland during Termination I (seesaw pattern) have been confirmed by ice cores (Severinghaus and Brook, 1999; Brook and Buizert, 2018; Stolper et al., 2016) and are attributed to changes in the intensity of the Atlantic Meridional Overturning Circulation (AMOC, Baker et al., 2009, 2010). The cooling of the Northern Hemisphere reduces the strength of the AMOC (Deaney et al., 2017; Muschitiello et al., 2019), which, in turn, causes the ventilation of the Southern Hemisphere oceans and the emission of

a large amount of CO<sub>2</sub> into the atmosphere, significantly warming Antarctica (Ahn et al., 2012; Beeman et al., 2019; Clementi and Sikes, 2019). Inverse temperatures between the two hemispheres during Termination I resulted in opposite behavior of the glaciers in each hemisphere (Jomelli et al., 2014; Darvill et al., 2016; Koffman et al., 2017; Shulmeister et al., 2019). However, this was not the case during the Holocene, mainly during Neoglaciation. The orbitally-forced changes in insolation are likely to be the main driver of Neoglaciation. In fact, negative Total Solar Irradiance anomalies are proposed as one of the main triggers of neoglacial advances into the large scale climatic transformations (Renssen et al., 2009; Solomina et al., 2015), together with volcanic activity, which also played an important role in some of the neoglacial events (Miller et al., 2012, 2013). Both the HTM and the Neoglaciation are global-scale patterns, despite recording notable regional variability. This could be the critical difference with the current warm period (RRW), where the response of glaciers is almost global and synchronous (Renssen et al., 2012; Solomina et al., 2015).

## 7. Conclusions

Establishing the chronology of deglaciation of ice-free areas in the AP region is of key importance in a changing climate scenario. To that purpose, we have reconstructed the calendar of the most recent glacial oscillations in the largest ice-free area in the SSI, the Byers Peninsula. Here, previous knowledge on the deglaciation was based on only a few radiocarbon dates from lake sediments that did not offer an accurate picture of the glacial evolution of the Mid-Late Holocene. We used CRE dating to examine the timing of neoglacial advances of Rotch Dome Glacier and compare it with other areas across the AP region.

Deglaciation of today's main ice-free areas in the SSI and the rest of the AP occurred between 9 and 6 ka, according to previous studies. After 6 ka, glaciers were similar or smaller than their present-day size in most of the AP. The first neoglacial advance in this area took place from ~5.5 ka, followed by a warm period between 4 and 2.8 ka. Subsequently until 1.0 ka, there was another period of generalized neoglacial advance in the AP. In the SSI, there was evidence of cold periods from 5.8 to 5.6, and from 2.7 cal ka BP from some paleoclimatic proxies, but the glacial response to those climate shifts was still unknown. This study confirms that, as in other areas of the AP, glacial advances also occurred in the SSI during these Neoglaciation cold periods in ~4.1 and 1.0 ka.

The recent synthesis of glacial evolution in the Arctic since the Mid-Holocene shows that there was even larger regional diversity with regards to the chronology of neoglacial advances. In the Arctic, the regional climate forcings determine climate trends that can lead to glacial advance within a global tendency to warming. However, millennial-scale patterns between the Arctic and the AP region seem to follow common trends. This timing revealed by the neoglacial landforms should be taken into account when looking for the origin of climate changes that caused Neoglaciation, which was practically synchronous in both polar areas. Consequently, although the objective of this work was not to examine the origin and causes of Neoglaciation, we provide new evidence supporting a global background for neoglacial advances beyond hemispheric-scale factors, which would have favored neoglacial advances with different time ranges in both Polar Regions.

## Credit author statement

**David Palacios:** Conceptualization, Formal analysis, Investigation, Investigation, Writing, Supervision, Funding acquisition, Methodology. **Jesus Ruiz-Fernández:** Conceptualization, Formal

analysis, Investigation, Writing, Supervision, Funding acquisition, Project administration, Methodology. **Marc Oliva:** Conceptualization, Formal analysis, Investigation, Investigation, Writing, Supervision, Funding acquisition, Methodology. **Nuria Andrés:** Conceptualization, Formal analysis, Investigation, Writing, Visualization, Methodology. **José M. Fernández-Fernández:** Conceptualization, Formal analysis, Investigation, Writing, Visualization, Methodology. **Irene Schimmelpfennig:** Exhaustive correction of the manuscript, Conceptualization, Formal analysis, Investigation, Writing. **Laetitia Leanni:** Formal analysis, Investigation, Methodology. **Benjamín González-Díaz:** Formal analysis, Investigation. **ASTER Team:** Formal analysis, Investigation, Writing, Methodology.

## Declaration of competing interest

The authors declare that they have no known competing financial interests or personal relationships that could have appeared to influence the work reported in this paper.

## Acknowledgements

This paper was supported by the projects CTM2016-77878-P and CGL2015-65813-R (Spanish Ministry of Economy and Competitiveness), and NUNANTAR (02/SAICT/2017-32002; Fundação para a Ciência e a Tecnologia, Portugal). It also complements the research topics examined in the project PALEOGREEN (CTM2017-87976-P; Spanish Ministry of Economy and Competitiveness). We also thank the Portuguese Polar Program for their support in organizing field logistics. The <sup>10</sup>Be and <sup>36</sup>Cl measurements were performed at the ASTER AMS national facility (CEREGE, Aix en Provence), which is supported by the INSU/CNRS and the ANR through the "Projets thématiques d'excellence" program for the "Equipements d'excellence" ASTER-CEREGE action and IRD. David Palacios thanks to the Institute of Alpine and Arctic Research, at the University of Colorado, the facilities provided to coordinate this work during his Fulbright Grant stay there in 2019. Marc Oliva is supported by the Ramón y Cajal Program (RYC-2015-17597) and the Research Group ANTALP (Antarctic, Arctic, Alpine Environments; 2017-SGR-1102). We thank Dr. Vincent Jomelli, Dr. Jan-Hendrik May one anonymous reviewers for their valuable suggestions that have greatly improved the paper.

## Appendix A. Supplementary data

Supplementary data associated with this article can be found, in the online version, at <https://doi.org/10.1016/j.quascirev.2020.106248>.

## References

- Abram, N.J., Mulvaney, R., Wolff, E.W., Triest, J., Kipfstuhl, S., Trusel, L.D., Arrowsmith, C., 2013. Acceleration of snow melt in an Antarctic Peninsula ice core during the twentieth century. *Nat. Geosci.* 6 (5), 404. <https://doi.org/10.1038/NGEO1787>.
- Abram, N.J., Mulvaney, R., Vimeuz, F., Phipps, S.J., Turner, J., England, M.H., 2014. Evolution of the southern annular mode during the past millennium. *Nat. Clim. Chang.* 4 564–569.
- Ahn, J., Brook, E.J., Schmittner, A., Kreuz, K., 2012. Abrupt change in atmospheric CO<sub>2</sub> during the last ice age. *Geophys. Res. Lett.* 39, L18711. <https://doi.org/10.1029/2012GL053018>.
- Alfaro, P., López-Martínez, J., Maestro, A., Galindo-Zaldívar, J., Durán-Valsero, J.J., Cuchí, J.A., 2010. Recent tectonic and morphostructural evolution of Byers peninsula (Antarctica): insight into the development of the south Shetland islands and Bransfield basin. *J. Iber. Geol.* 36 (1), 21–38.
- Allen, C.S., Oakes-Fretwell, L., Anderson, J.B., Hodgson, D.A., 2010. A record of Holocene glacial and oceanographic variability in Neny fjord, antarctic peninsula. *Holocene* 20 (4), 551–564. <https://doi.org/10.1177/0959683609356581>.
- Anderson, J.T., Wilson, G.S., Fink, D., Lilly, K., Levy, R.H., Townsend, D., 2017. Reconciling marine and terrestrial evidence for post LGM ice sheet retreat in

- southern McMurdo Sound, Antarctica. *Quat. Sci. Rev.* 157, 1–13. <https://doi.org/10.1016/j.quascirev.2016.12.007>.
- Araya, R., Hervé, F., 1966. Estudio geomorfológico y geológico en las Islas Shetland del Sur Antártica, N° 8. Instituto Antártico Chileno, Santiago, Chile, p. 76.
- Arche, A., López-Martínez, J., Serrano, J., Martínez De Pisón, E., 1996. Marine landforms and deposits. In: López-Martínez, J., Thomson, M.R.A., Thomson, J.W. (Eds.), *Geomorphological Map of Byers Peninsula, Livingston Island. BAS GEOMAP Series, Sheet 5-a, 1:25 000, with Supplementary Text. British Antarctic Survey, Cambridge*, pp. 35–42.
- Arnold, M., Merchel, S., Bourlès, D.L., Braucher, R., Benedetti, L., Finkel, R.C., Aumaître, G., Gottsdang, A., Klein, M., 2010. The French accelerator mass spectrometry facility ASTER: improved performance and developments. Nuclear instruments and methods in physics research, section B, beam interactions with materials and atoms. In: 19th International Conference on Ion Beam Analysis, 268, pp. 1954–1959. <https://doi.org/10.1016/j.nimb.2010.02.107>.
- Balco, G., Schafer, J.M., LARISSA group, 2013. Exposure-age record of Holocene ice sheet and ice shelf change in the northeast Antarctic Peninsula. *Quat. Sci. Rev.* 59, 101–111. <https://doi.org/10.1016/j.quascirev.2012.10.022>.
- Balco, G., Stone, J.O., Sliwinski, M.G., Todd, C., 2014. Features of the glacial history of the Transantarctic Mountains inferred from cosmogenic <sup>26</sup>Al, <sup>10</sup>Be and <sup>21</sup>Ne concentrations in bedrock surfaces. *Antarct. Sci.* 26 (6), 708–723. <https://doi.org/10.1017/S0954102014000261>.
- Bañón, M., Justel, A., Velázquez, D., Quesada, A., 2013. Regional weather survey on Byers peninsula, Livingston island, South Shetland islands, Antarctica. *Antarct. Sci.* 25 (2), 146–156. <https://doi.org/10.1017/S0954102012001046>.
- Barker, S., Diz, P., Vautravers, M.J., Pike, J., Knorr, G., Hall, I.R., Broecker, W.S., 2009. Interhemispheric Atlantic seesaw response during the last deglaciation. *Nature* 457 (7233), 1097.
- Barker, S., Knorr, G., Vautravers, M.J., Diz, P., Skinner, L.C., 2010. Extreme deepening of the Atlantic overturning circulation during deglaciation. *Nat. Geosci.* 3 (8), 567.
- Barnard, A., Wellner, J.S., Anderson, J.B., 2014. Late Holocene climate change recorded in proxy records from a Bransfield Basin sediment core, Antarctic Peninsula. *Polar Res.* 33 (1), 17236. <https://doi.org/10.3402/polar.v33.17236>.
- Barsch, D., Mäusbacher, R., 1986. New data on the relief development of the south Shetland islands, Antarctica. *Interdiscipl. Sci. Rev.* 11 (2), 211–218. <https://doi.org/10.1179/isr.1986.11.2.211>.
- Beeman, C.J., Gest, L., Parrenin, F., Raynaud, D., Fudge, T.J., Buizert, C., Brook, E.J., 2019. Antarctic temperature and CO<sub>2</sub>: near-synchrony yet variable phasing during the last deglaciation. *Clim. Past* 15, 913–926. <https://doi.org/10.5194/cp-15-913-2019>.
- Benayas, J., Pertierra, L., Tejado, P., Lara, F., Bermudez, O., Hughes, K.A., Quesada, A., 2013. A review of scientific research trends within ASPA no. 126 Byers Peninsula, South Shetland Islands, Antarctica. *Antarct. Sci.* 25 (2), 128–145.
- Bentley, M.J., Hodgson, D.A., 2009. Antarctic ice sheet and climate history since the last glacial maximum. *PAGES News* 17 (1), 28–29.
- Bentley, M.J., Hodgson, D.A., Smith, J.A., Cox, N.J., 2005. relative sea level curves for the south Shetland islands and marguerite bay, antarctic peninsula. *Quat. Sci. Rev.* 24 (10–11), 1203–1216. <https://doi.org/10.1016/j.quascirev.2004.10.004>.
- Bentley, M.J., Hodgson, D.A., Smith, J.A., Cofaigh, C.O., Domack, E.W., Larter, R.D., Hillenbrand, C.D., 2009. Mechanisms of Holocene palaeoenvironmental change in the antarctic peninsula region. *Holocene* 19 (1), 51–69. <https://doi.org/10.1177/0959683608096603>.
- Bentley, M.J., Cofaigh, C.O., Anderson, J.B., Conway, H., Davies, B., Graham, A.G., Mackintosh, A., 2014. A community-based geological reconstruction of antarctic ice sheet deglaciation since the last glacial maximum. *Quat. Sci. Rev.* 100, 1–9. <https://doi.org/10.1016/j.quascirev.2014.06.025>.
- Bertler, N.A.N., Mayewski, P.A., Carter, L., 2011. Cold conditions in Antarctica during the Little Ice Age e implications for abrupt climate change mechanisms. *Earth Planet. Sci. Lett.* 308, 41–51. <https://doi.org/10.1016/j.epsl.2011.05.021>.
- Birkenmajer, K., 1981. Raised marine features and glacial history in the vicinity of H. Arctowski station, king George island (South Shetland islands, west Antarctica). *Bull. Pol. Acad. Sci.* 29, 109–117.
- Birkenmajer, K., 1995. glacier retreat and raised marine beaches at three sisters Point, king George island (South Shetland islands, west Antarctica). *Bull. Pol. Acad. Sci.* 43, 135–141.
- Birkenmajer, K., 1998. Quaternary geology at potter peninsula, king George island (South Shetland islands, west Antarctica). *Bull. Pol. Acad. Sci.* 46, 9–20.
- Birkenmajer, K., 2002. Retreat of ecology glacier, admiralty bay, king George island (South Shetland islands, west Antarctica), 1956–2001. *Bull. Pol. Acad. Sci.* 50, 15–29.
- Björck, S., Hakansson, H., Zale, R., Karlén, W., Jónsson, B.L., 1991. A late Holocene lake sediment sequence from Livingston Island, South Shetland Islands, with palaeoclimatic implications. *Antarct. Sci.* 3, 61–72.
- Björck, S., Hakansson, H., Olsson, S., Barnekow, L., Janssens, J., 1993. Palaeoclimatic studies in South Shetlands Islands, Antarctica, based on numerous stratigraphic variables in lake sediments. *J. Paleolimnol.* 8, 233–272.
- Björck, S., Olsson, S., Ellis-Evans, C., Hakansson, H., Humlum, O., de Lirio, J.M., 1996a. Late Holocene palaeoclimatic records from lake sediments on James Ross island, Antarctica. *Palaeogeogr., Palaeoclimat., Palaeoecol.* 121 (3–4), 195–220.
- Björck, S., Hjort, C., Ingólfsson, Ó., Zale, R., Ising, J., 1996b. Holocene glacial chronology from lake sediments. In: López-Martínez, J., Thomson, M.R.A., Thomson, J.W. (Eds.), *Geomorphological Map of Byers Peninsula, Livingston Island. BAS GEOMAP Series, Sheet 5-a, 1:25 000, with Supplementary Text. British Antarctic Survey, Cambridge*, pp. 49–51.
- Braucher, R., Guillou, V., Bourlès, D.L., Arnold, M., Aumaître, G., Keddadouche, K., Nottoli, E., 2015. Preparation of ASTER in-house <sup>10</sup>Be/<sup>9</sup>Be standard solutions. Nuclear instruments and methods in physics research, section B, beam interactions with materials and atoms. In: The Thirteenth Accelerator Mass Spectrometry Conference, vol. 361, pp. 335–340. <https://doi.org/10.1016/j.nimb.2015.06.012>.
- Brightley, H., 2017. A paleoclimate reconstruction of the Little ice age to modern Era climate conditions in the eastern Ross Sea, Antarctica as captured in the RICE ice core. A thesis submitted to Victoria University of Wellington in partial fulfilment of the requirements for the degree of Master of Science in Geology. In: School of Geography, Environmental and Earth Sciences, Victoria University of Wellington. <http://hdl.handle.net/10063/6394>.
- Briner, J.P., McKay, N.P., Axford, Y., Bennike, O., Bradley, R.S., de Vernal, A., Jennings, A., 2016. Holocene climate change in Arctic Canada and Greenland. *Quat. Sci. Rev.* 147, 340–364.
- Broecker, W.S., Denton, G.H., 1990. The role of ocean-atmosphere reorganizations in glacial cycles. *Quat. Sci. Rev.* 9, 305–341.
- Brook, E.J., Buizert, C., 2018. Antarctic and global climate history viewed from ice cores. *Nature* 558 (7709), 200.
- Carrivick, J.L., Davies, B.J., Glasser, N.F., Nývlt, D., 2012. Late Holocene changes in character and behaviour of land-terminating glaciers on James Ross Island, Antarctica. *J. Glaciol.* 58, 1176–1190. <https://doi.org/10.3189/2012jog11j148>.
- Čejka, T., Nývlt, D., Kopalová, K., Bulínová, M., Kavan, J., Lirio, J.M., Coria, S.H., van de Vijver, B., 2019. Timing of the neoglaciation onset on the North-eastern antarctic peninsula based on lacustrine archive from lake anónima, Vega island. *Global Planet. Change* 184. <https://doi.org/10.1016/j.gloplacha.2019.103050>.
- Charman, D.J., Amesbury, M.J., Roland, T.P., Royles, J., Hodgson, D.A., Convey, P., Griffiths, H., 2013. Spatially coherent late Holocene Antarctic Peninsula surface air temperature variability. *Geology* 46, 1071–1074. <https://doi.org/10.1130/G45347.1>.
- Chmieleff, J., von Blanckenburg, F., Kossert, K., Jakob, D., 2010. Determination of the <sup>10</sup>Be half-life by multicollector ICP-MS and liquid scintillation counting nuclear instruments and methods in physics research, section B. *Beam Interact. Mater. Atoms* 268, 192–199. <https://doi.org/10.1016/j.nimb.2009.09.012>.
- Christ, A.J., Talaia-Murray, M., Elking, N., Domack, E.W., Leventer, A., Lavoie, C., Petrushak, S., 2015. Late Holocene glacial advance and ice shelf growth in Barilari bay, Graham land, west antarctic peninsula. *GSA Bulletin* 127 (1–2), 297–315. <https://doi.org/10.1130/B31035.1>.
- Chu, Z., Sun, L., Wang, Y., Huang, T., Zhou, X., 2017. Depositional environment and climate changes during the Holocene in grande valley, Fildes peninsula, king George island, Antarctica. *Antarct. Sci.* 29 (6), 545–554. <https://doi.org/10.1017/S095410201700030X>.
- Çiner, A., Yildirim, C., Sarikaya, M.A., Seong, Y.B., Yu, B.Y., 2019. Cosmogenic <sup>10</sup>Be exposure dating of glacial erratics on Horseshoe Island in western Antarctic Peninsula confirms rapid deglaciation in the Early Holocene. *Antarct. Sci.* 31 (6), 319–331. <https://doi.org/10.1017/S0954102019000439>.
- Clapperton, C.M., Sugden, D.E., 1988. Holocene glacier fluctuations in South America and Antarctica. *Quat. Sci. Rev.* 7 (2), 185–198.
- Clapperton, C.M., Sugden, D.E., Birnie, J., Wilson, M.J., 1989. Late-glacial and Holocene glacier fluctuations and environmental change on South Georgia, Southern Ocean. *Quat. Res.* 31 (2), 210–228. [https://doi.org/10.1016/0033-5894\(89\)90006-9](https://doi.org/10.1016/0033-5894(89)90006-9).
- Clementi, V.J., Sikes, E.L., 2019. Southwest Pacific vertical structure influences on oceanic carbon storage since the Last Glacial Maximum. *Paleoceanogr. Paleoclim.* 34, 734–754. <https://doi.org/10.1029/2018PA003501>.
- Cofaigh, C.O., Davies, B.J., Livingstone, S.J., Smith, J.A., Johnson, J.S., Hocking, E.P., Domack, E., 2014. Reconstruction of ice-sheet changes in the antarctic peninsula since the last glacial maximum. *Quat. Sci. Rev.* 100, 87–110. <https://doi.org/10.1016/j.quascirev.2014.06.023>.
- Cook, A.J., Fox, A.J., Vaughan, D.G., Ferrigno, J.G., 2005. Retreating glacier fronts on the Antarctic Peninsula over the past half-century. *Science* 308 (5721), 541–544. <https://doi.org/10.1126/science.1104235>.
- Correia, A., Oliva, M., Ruiz-Fernández, J., 2017. Evaluation of frozen ground conditions along a coastal topographic gradient at Byers Peninsula (Livingston Island, Antarctica) by geophysical and geoeological methods. *Catena* 149, 529–537. <https://doi.org/10.1016/j.catena.2016.06.006>.
- Curl, J.E., 1980. A Glacial History of the South Shetland Islands, Antarctica. Institute of Polar Studies, Intitute of Polar Studies, Report N° 63. The Ohio State University, p. 129.
- Darvill, C.M., Bentley, M.J., Stokes, C.R., Shulmeister, J., 2016. The timing and cause of glacial advances in the southern mid-latitudes during the last glacial cycle based on a synthesis of exposure ages from Patagonia and New Zealand. *Quat. Sci. Rev.* 149, 200–214.
- Davies, B.J., Hambrey, M.J., Smellie, J.L., Carrivick, J.L., Glasser, N.F., 2012. Antarctic peninsula ice sheet evolution during the cenozoic Era. *Quat. Sci. Rev.* 31, 30–66. <https://doi.org/10.1016/j.quascirev.2011.10.012>.
- Davies, B.J., Glasser, N.F., Carrivick, J.L., Hambrey, M.J., Smellie, J.L., Nývlt, D., 2013. Landscape evolution and ice-sheet behaviour in a semi-arid polar environment: James Ross island, NE antarctic peninsula. *Geol. Soc., Lond., Spec. Publ.* 381 (1), 353–395. <https://doi.org/10.1144/SP381.1>.
- Davies, B.J., Gollledge, N.R., Glasser, N.F., Carrivick, J.L., Ligtenberg, S.R., Barrand, N.E., Smellie, J.L., 2014. Modelled glacier response to centennial temperature and precipitation trends on the Antarctic Peninsula. *Nat. Clim. Change* 4 (11), 993. <https://doi.org/10.1038/NCLIMATE2369>.
- Davies, B.J., Hambrey, M.J., Glasser, N.F., Holt, T., Rodés, A., Smellie, J.L., Blockley, S.P.,

2017. Ice-dammed lateral lake and epishelf lake insights into Holocene dynamics of marguerite trough ice stream and George VI ice shelf, alexander island, antarctic peninsula. *Quat. Sci. Rev.* 177, 189–219. <https://doi.org/10.1016/j.quascirev.2017.10.016>.
- De Pablo, M.A., Ramos, M., Molina, A., 2014. Thermal characterization of the active layer at the limnopolare lake CALM-S site on Byers peninsula (Livingston island), Antarctica. *Solid Earth* 5 (2), 721–739. <https://doi.org/10.5194/se-5-721-2014>.
- Deaney, E.L., Barker, S., Van De Fliert, T., 2017. Timing and nature of AMOC recovery across Termination 2 and magnitude of deglacial CO<sub>2</sub> change. *Nat. Commun.* 8, 14595.
- Del Valle, R.A., Montalti, D., Inbar, M., 2002. Mid-holocene macrofossil-bearing raised marine beaches at potter peninsula, king George island, South Shetland islands. *Antarct. Sci.* 14 (3), 263–269. <https://doi.org/10.1017/S0954102002000081>.
- Domack, E., Ishman, S., Stein, A.B., McClennen, C.E., Jull, A.J.T., 1995. Late Holocene advance of Müller ice shelf, antarctic peninsula: sedimentological, geochemical, and palaeontological evidence. *Antarct. Sci.* 7, 159–170.
- Domack, E.W., Leventer, A., Dunbar, G.B., Taylor, F., Brachfeld, S., Sjunneskog, C., Party, O.L.S., 2001. Chronology of the palmer deep site, antarctic peninsula: a Holocene palaeoenvironmental reference for the circum-antarctic. *Holocene* 11, 1–9.
- Dunai, T.J., 2010. *Cosmogenic Nuclides*. Cambridge University Press, Cambridge. <https://doi.org/10.1017/CBO9780511804519>.
- Engel, Z., Láska, K., Nývlt, D., Stachoň, Z., 2018. Surface mass balance of small glaciers on James Ross island, north-eastern antarctic peninsula, during 2009–2015. *J. Glaciol.* 64 (245), 349–361.
- Everett, K.R., 1971. Observations on the glacial history of Livingston island. *Arctic* 41–50.
- Fink, D., Vogt, S., Hotchkis, M., 2000. Cross-sections for <sup>36</sup>Cl from Ti at Ep=35–150 MeV: applications to in-situ exposure dating. *Nucl. Instruments methods phys. Res. Sect. B beam interact. With mater. Atoms* 172, 861–866. [https://doi.org/10.1016/S0168-583X\(00\)00200-7](https://doi.org/10.1016/S0168-583X(00)00200-7).
- Fretwell, P.T., Hodgson, D.A., Watcham, E.P., Bentley, M.J., Roberts, S.J., 2010. Holocene isostatic uplift of the south Shetland islands, antarctic peninsula, modelled from raised beaches. *Quat. Sci. Rev.* 29 (15–16), 1880–1893. <https://doi.org/10.1016/j.quascirev.2010.04.006>.
- Geirsdóttir, A., Miller, G.H., Andrews, J.T., Harning, D.J., Anderson, L.S., Florian, C., Thordarson, T., 2019. The onset of neoglaciation in Iceland and the 4.2 ka event. *Clim. Past* 15 (1), 25–40. <https://doi.org/10.5194/cp-15-25-2019>.
- Glasser, N.F., Davies, B.J., Carrivick, J.L., Rodés, A., Hambrey, M.J., Smellie, J.L., Domack, E., 2014. Ice-stream initiation, duration and thinning on James Ross island, northern antarctic peninsula. *Quat. Sci. Rev.* 86, 78–88. <https://doi.org/10.1016/j.quascirev.2013.11.012>.
- Guglielmin, M., Convey, P., Malfasi, F., Cannone, N., 2016. Glacial fluctuations since the 'medieval warm period' at Rothera Point (western antarctic peninsula). *Holocene* 26 (1), 154–158. <https://doi.org/10.1177/0959683615596827>.
- Hall, B.L., 2003. An overview of late pleistocene glaciation in the south Shetland islands. *Antarct. Res.* 79, 103–113. <https://doi.org/10.1029/079ARS09>.
- Hall, B.L., 2007. Late-holocene advance of the Collins ice cap, king George island, South Shetland islands. *Holocene* 17 (8), 1253–1258. <https://doi.org/10.1177/0959683607085132>.
- Hall, B.L., 2009. Holocene glacial history of Antarctica and the sub-Antarctic islands. *Quat. Sci. Rev.* 28 (21–22), 2213–2230. <https://doi.org/10.1016/j.quascirev.2009.06.011>.
- Hall, B.L., 2010. Holocene relative sea-level changes and ice fluctuations in the South Shetland Islands. *Global Planet. Change* 74, 15–26.
- Hall, B.L., Denton, G.H., 1999. New relative sea-level curves for the southern Scott Coast, Antarctica: evidence for Holocene deglaciation of the western Ross Sea. *J. Quat. Sci.* 14 (7), 641–650.
- Hall, B.L., Denton, G., 2002. Holocene history of the Wilson Piedmont glacier along the southern Scott coast. *Holocene* 12, 619–627. <https://doi.org/10.1191/0959683602hl572rp>.
- Hall, B.L., Perry, E.R., 2004. Variations in ice rafted detritus on beaches in the South Shetland Islands: a possible climate proxy. *Antarct. Sci.* 16 (3), 339–344. <https://doi.org/10.1017/S09541020040002147>.
- Hall, B.L., Koffman, T., Denton, G.H., 2010. Reduced ice extent on the western Antarctic Peninsula at 700–970 cal. yr BP. *Geology* 38 (7), 635–638. <https://doi.org/10.1130/G30932.1>.
- Hambrey, M.J., Davies, B.J., Glasser, N.F., Holt, T.O., Smellie, J.L., Carrivick, J.L., 2015. Structure and sedimentology of George VI Ice Shelf, Antarctic Peninsula: implications for ice-sheet dynamics and landform development. *J. Geol. Soc.* 172 (5), 599–613. <https://doi.org/10.1144/jgs2014-134>.
- Hansom, J.D., 1979. Radiocarbon dating of a raised beach at 10 m in the south Shetland islands. *Br. Antarct. Surv. Bull.* 49, 287–288.
- Hathway, B., Lomas, S.A., 1998. The upper Jurassic-lower cretaceous Byers group, South Shetland islands, Antarctica: revised stratigraphy and regional correlations. *Cretac. Res.* 19, 43–67.
- Heroy, D.C., Sjunneskog, C., Anderson, J.B., 2008. Holocene climate change in the Bransfield Basin, Antarctic Peninsula: evidence from sediment and diatom analysis. *Antarct. Sci.* 20 (1), 69–87. <https://doi.org/10.1017/S0954102007000788>.
- Hodgson, D.A., Roberts, S.J., Smith, J.A., Verleyen, E., Sterken, M., Labarque, M., Bryant, C., 2013. Late Quaternary environmental changes in Marguerite Bay, Antarctic Peninsula, inferred from lake sediments and raised beaches. *Quat. Sci. Rev.* 68, 216–236. <https://doi.org/10.1016/j.quascirev.2011.10.011>.
- Hrbáček, F., Oliva, M., Láska, K., Ruiz-Fernandez, J., de Pablo, M.A., Vieira, G., Ramos, M., Nývlt, D., 2016. Active layer thermal regime in two climatically contrasted sites of the Antarctic Peninsula region. *Cuadernos de Investigación Geográfica* 42 (2), 457–474.
- Ingólfsson, Ó., Hjort, C., Berkman, P.A., Björck, S., Colhoun, E., Goodwin, I.D., Prentice, M.L., 1998. Antarctic glacial history since the Last Glacial Maximum: an overview of the record on land. *Antarct. Sci.* 10 (3), 326–344.
- Ingólfsson, Ó., Hjort, C., Humlum, O., 2003. Glacial and climate history of the antarctic peninsula since the last glacial maximum. *Arctic Antarct. Alpine Res.* 35 (2), 175–186. [https://doi.org/10.1657/1523-0430\(2003\)035\[0175:GACHOT\]2.0.CO;2](https://doi.org/10.1657/1523-0430(2003)035[0175:GACHOT]2.0.CO;2).
- Ivy-Ochs, S., Synal, H.-A., Roth, C., Schaller, M., 2004. Initial results from isotope dilution for Cl and <sup>36</sup>Cl measurements at the PSI/ETH Zurich AMS facility. *Nucl. Inst. Methods Phys. Res. Sect. B Beam Interact. Mater. Atoms* 223–224, 623–627. <https://doi.org/10.1016/j.nimb.2004.04.115>.
- John, B.S., 1972. Evidence from the south Shetland islands towards a glacial history of west Antarctica. *Institute of British geographers. Spec. Publ.* 4, 75–89.
- John, B.S., Sugden, D.E., 1971. Raised marine features and phases of glaciation in the South Shetland Islands. *Br. Antarct. Surv. Bull.* 24, 45–111.
- Jomelli, V., Favier, V., Vuille, M., Braucher, R., Martin, L., Blard, P.H., Colose, C., Brunstein, D., He, F., Khodri, M., Bourles, D.L., Leanni, L., Rinterknecht, V., Grancher, D., Franco, B., Ceballos, J.L., Fonseca, H., Liu, Z., Otto-Bliesner, B.L., 2014. A major advance of tropical Andean glaciers during the Antarctic cold reversal. *Nature* 513, 224–228.
- Kaplan, M.R., Strelin, J.A., Schaefer, J.M., Peltier, C., Martini, M.A., Flores, E., Winckler, G., Schwartz, R., 2020. Holocene glacier behavior around the northern Antarctic Peninsula and possible causes. *Earth Planet. Sci. Lett.* 534 (116077) <https://doi.org/10.1016/j.epsl.2020.116077>.
- Kaufman, D.S., Ager, T.A., Anderson, N.J., Anderson, P.M., Andrews, J.T., Bartlein, P.J., Dyke, A.S., 2004. Holocene thermal maximum in the western Arctic (0–180 W). *Quat. Sci. Rev.* 23 (5–6), 529–560. <https://doi.org/10.1016/j.quascirev.2003.09.007>.
- Kaufman, D.S., Axford, Y.L., Henderson, A.C., McKay, N.P., Oswald, W.W., Saenger, C., Hu, F.S., 2016. Holocene climate changes in eastern Beringia (NW North America)—A systematic review of multi-proxy evidence. *Quat. Sci. Rev.* 147, 312–339.
- Khim, B.K., Yoon, H.I., Kang, C.Y., Bahk, J.J., 2002. Unstable climate oscillations during the late Holocene in the eastern Bransfield basin, antarctic peninsula. *Quat. Res.* 58, 234–245. <https://doi.org/10.1006/qres.2002.2371>.
- Koffman, T.N., Schaefer, J.M., Putnam, A.E., Denton, G.H., Barrell, D.J., Rowan, A.V., Brocklehurst, S.H., 2017. A beryllium-10 chronology of late-glacial moraines in the upper Rakaia valley, Southern Alps, New Zealand supports Southern-Hemisphere warming during the Younger Dryas. *Quat. Sci. Rev.* 170, 14–25.
- Korschinek, G., Bergmaier, A., Faestermann, T., Gerstmann, U.C., Knie, K., Rugel, G., Wallner, A., Dillmann, I., Dollinger, G., von Gostomski, C.L., Kossert, K., Maiti, M., Poutivtsev, M., Remmert, A., 2010. A new value for the half-life of <sup>10</sup>Be by heavy-ion elastic recoil detection and liquid scintillation counting. *Nuclear instruments and methods in physics research, section B, Beam Interact. Mater. Atoms* 268, 187–191. <https://doi.org/10.1016/j.nimb.2009.09.020>.
- Kunz, M., King, M.A., Mills, J.P., Miller, P.E., Fox, A.J., Vaughan, D.G., Marsh, S.H., 2012. Multi-decadal glacier surface lowering in the antarctic peninsula. *Geophys. Res. Lett.* 39 (19), 1–5.
- Larter, R.D., Anderson, J.B., Graham, A.G., Gohl, K., Hillenbrand, C.D., Jakobsson, M., Witus, A.E., 2014. Reconstruction of changes in the Amundsen Sea and Bellingshausen sea sector of the West Antarctic ice sheet since the last glacial maximum. *Quat. Sci. Rev.* 100, 55–86. <https://doi.org/10.1016/j.quascirev.2013.10.016>.
- Li, Y., Cole-Dai, J., Zhou, L., 2009. Glaciochemical evidence in an East Antarctica ice core of a recent (AD 1450–1850) neoglaciation episode. *J. Geophys. Res.: Atmospheres* 114 (D8), 1–11. <https://doi.org/10.1029/2008JD011091>.
- Lifton, N., Sato, T., Dunai, T.J., 2014. Scaling in situ cosmogenic nuclide production rates using analytical approximations to atmospheric cosmic-ray fluxes. *Earth Planet. Sci. Lett.* 386, 149–160. <https://doi.org/10.1016/j.epsl.2013.10.052>.
- Lindsay, D.C., 1971. Vegetation of the south Shetland islands. *Br. Antarct. Surv. Bull.* 25, 59–83.
- López-Martínez, J., Martínez de Pisón, E., Arche, A., 1992. Geomorphology of Hurd peninsula, Livingston island, South Shetland islands. In: Yoshida, Y., Kaminuma, K., Shiraishi, K. (Eds.), *Recent Progress in Antarctic Earth Science*. Terra Scientific Publishing Company, Tokyo, pp. 751–756.
- López-Martínez, J., Serrano, E., Schmid, T., Mink, S., Linés, C., 2012. Periglacial processes and landforms in the south Shetland islands (northern antarctic peninsula region). *Geomorphology* 155/156, 62–79.
- López-Martínez, J., Thomson, M.R.A., Thomson, J.W., 1996. Geomorphological map of Byers Peninsula, Livingston Island. *BAS GEOMAP Series, Sheet 5-A, Scale 1:25 000 with supplementary text*. British Antarctic Survey, Cambridge, p. 65.
- Lorius, C., Jouzel, J., Raynaud, D., Hansen, J., Le Treut, H., 1990. The ice-core record: climate sensitivity and future greenhouse warming. *Nature* 347 (6289), 139–145.
- Mackintosh, A., Gollidge, N., Domack, E., Dunbar, R., Leventer, A., White, D., Gore, D., 2011. Retreat of the East Antarctic ice sheet during the last glacial termination. *Nat. Geosci.* 4 (3), 195. <https://doi.org/10.1038/NNGEO1061>.
- Mackintosh, A.N., Verleyen, E., O'Brien, P.E., White, D.A., Jones, R.S., McKay, R., Miura, H., 2014. Retreat history of the east antarctic ice sheet since the last glacial maximum. *Quat. Sci. Rev.* 100, 10–30. <https://doi.org/10.1016/j.quascirev.2013.07.024>.

- Marcott, S.A., Shakun, J.D., Clark, P.U., Mix, A.C., 2013. A reconstruction of regional and global temperature for the past 11,300 years. *Science* 339 (6124), 1198–1201. <https://doi.org/10.1126/science.1228026>.
- Marrero, S.M., Phillips, F.M., Caffee, M.W., Gosse, J.C., 2016. CRONUS – earth cosmogenic <sup>36</sup>Cl calibration. *Quat. Geochronol.* 31, 199–219. <https://doi.org/10.1016/j.quageo.2015.10.002>.
- Martin, L.C.P., Blard, P.-H., Balco, G., Lavé, J., Delunel, R., Lifton, N., Laurent, V., 2017. The CREP program and the ICE-D production rate calibration database: a fully parameterizable and updated online tool to compute cosmic-ray exposure ages. *Quat. Geochronol.* 38, 25–49. <https://doi.org/10.1016/j.quageo.2016.11.006>.
- Martínez De Pisón, E., Serrano, E., Arche, A., López-Martínez, J., 1996. Glacial geomorphology. In: López-Martínez, J., Thomson, M.R.A., Thomson, J.W. (Eds.), *Geomorphological Map of Byers Peninsula, Livingston Island. BAS GEOMAP Series, Sheet 5-a, 1:25000, with Supplementary Text. British Antarctic Survey, Cambridge*, pp. 23–27.
- Mäusbacher, R., 1991. Die jungquartäre Relief- und Klimageschichte im Bereich der Fildeshalbinsel Süd-Shetland-Inseln, Antarktis. Ph.D. dissertation. Geographisches Institut der Universität Heidelberg, p. 382.
- Mäusbacher, R., Müller, J., Schmidt, R., 1989. Evolution of postglacial sedimentation in antarctic lakes (king George island). *Zeitschrift Fur Geomorphologie* 33 (2), 219–234.
- McKay, N.P., Kaufman, D.S., Routson, C.C., Erb, M.P., Zander, P.D., 2018. The onset and rate of Holocene Neoglacial cooling in the Arctic. *Geophys. Res. Lett.* 45 (22), 12–487. <https://doi.org/10.1029/2018GL079773>.
- Merchel, S., Herpers, U., 1999. An update on radiochemical separation techniques for the determination of long-lived radionuclides via accelerator mass spectrometry. *Radiochim. Acta* 84 (4), 215–220.
- Merchel, S., Arnold, M., Aumaitre, G., Benedetti, L., Bourlès, D.L., Braucher, R., Alfimov, V., Freeman, S.P.H.T., Steier, P., Wallner, A., 2008. Towards more precise <sup>10</sup>Be and <sup>36</sup>Cl data from measurements at the 10–14 level: influence of sample preparation. *Nuclear Instruments and Methods in Physics Research, Section B. Beam Interact. Mater. Atoms* 266, 4921–4926. <https://doi.org/10.1016/j.nimb.2008.07.031>.
- Merchel, S., Bremser, W., Alfimov, V., Arnold, M., Aumaitre, G., Benedetti, L., Bourlès, D.L., Caffee, M., Fifield, L.K., Finkel, R.C., Freeman, S.P.H.T., Martschini, M., Matsushi, Y., Rood, D.H., Sasa, K., Steier, P., Takahashi, T., Tamari, M., Tims, S.G., Tosaki, Y., Wilcken, K.M., Xu, S., 2011. Ultra-trace analysis of <sup>36</sup>Cl by accelerator mass spectrometry: an interlaboratory study. *Anal. Bioanal. Chem.* <https://doi.org/10.1007/s00216-011-4979-2>.
- Michalchuk, B.R., Anderson, J.B., Wellner, J.S., Manley, P.L., Majewski, W., Bohaty, S., 2009. Holocene climate and glacial history of the northeastern Antarctic Peninsula: the marine sedimentary record from a long SHALDRIL core. *Quat. Sci. Rev.* 28 (27–28), 3049–3065. <https://doi.org/10.1016/j.quascirev.2009.08.012>.
- Miller, G.H., Geirsdóttir, Á., Zhong, Y., Larsen, D.J., Otto-Bliesner, B.L., Holland, M.M., Bailey, D.A., Refsnider, K.A., Lehman, S.J., Southon, J.R., Anderson, C., Björnsson, H., Thordarson, T., 2012. Abrupt onset of the Little Ice Age triggered by volcanism and sustained by sea-ice/ocean feedbacks. *Geophys. Res. Lett.* 39, L02708. <https://doi.org/10.1029/2011GL051068>.
- Miller, G.H., Lehman, S.J., Refsnider, K.A., Southon, J.R., Zhong, Y., 2013. Unprecedented recent summer warmth in Arctic Canada. *Geophys. Res. Lett.* 40, 5745–5751. <https://doi.org/10.1002/2013GL057188>.
- Miller, G.H., Landvik, J.Y., Lehman, S.J., Southon, J.R., 2017. Episodic Neoglacial snowline descent and glacier expansion on Svalbard reconstructed from the 14C ages of ice-entombed plants. *Quat. Sci. Rev.* 155, 67–78.
- Milliken, K.T., Anderson, J.B., Wellner, J.S., Bohaty, S.M., Manley, P.L., 2009. High-resolution Holocene climate record from Maxwell bay, South Shetland islands, Antarctica. *Holocene climate record from Maxwell bay. GSA Bulletin* 121 (11–12), 1711–1725.
- Mosley-Thompson, E., 1996. Holocene climate changes recorded in an East Antarctica ice core. Climatic variations and forcing mechanisms of the last 2,000. In: Jones, P.D., Bradley, R., Jouzel, J. (Eds.), *NATO Advanced Research Series I, vol. 41*, pp. 263–279.
- Mosley-Thompson, E., Thompson, L.G., Grootes, P.M., Gundestrup, N., 1990. Little ice age (neoglacial) paleoenvironmental conditions at siple station, Antarctica. *Ann. Glaciol.* 14, 199–204.
- Muschitiello, F., D'Andrea, W.J., Schmittner, A., Heaton, T.J., Balascio, N.L., Caffee, M.W., Dokken, T.M., 2019. Deep-water circulation changes lead North Atlantic climate during deglaciation. *Nat. Commun.* 10 (1), 1272.
- Navarro, F., Jonsell, U., Corcuera, M.I., Martín Español, A., 2013. Decelerated mass loss of Hurd and Johnsons glaciers, Livingston island, antarctic peninsula. *J. Glaciol.* 59 (213), 115–128.
- Oliva, M., Ruiz-Fernández, J., 2015. Coupling patterns between para-glacial and permafrost degradation responses in Antarctica. *Earth Surf. Process. Landforms* 40 (9), 1227–1238. <https://doi.org/10.1002/esp.3716>.
- Oliva, M., Ruiz-Fernández, J., 2017. Geomorphological processes and frozen ground conditions in elephant Point (Livingston island, South Shetland islands, Antarctica). *Geomorphology* 293, 368–379. <https://doi.org/10.1016/j.geomorph.2016.01.020>.
- Oliva, M., Antoniades, D., Giral, S., Granados, I., Pla-Rabes, S., Toro, M., Liu, E.J., Sanjurjo, J., Vieira, G., 2016. The Holocene deglaciation of the Byers Peninsula (Livingston Island, Antarctica) based on the dating of lake sedimentary records. *Geomorphology* 261, 89–102. <https://doi.org/10.1016/j.geomorph.2016.02.029>.
- Oliva, M., Navarro, F., Hrbáček, F., Hernández, A., Nývlt, D., Pereira, P., Trigo, R., 2017a. Recent regional climate cooling on the Antarctic Peninsula and associated impacts on the cryosphere. *Sci. Total Environ.* 580, 210–223. <https://doi.org/10.1016/j.scitotenv.2016.12.030>.
- Oliva, M., Hrbáček, F., Ruiz-Fernández, J., de Pablo, M.Á., Vieira, G., Ramos, M., Antoniades, D., 2017b. Active layer dynamics in three topographically distinct lake catchments in Byers Peninsula (Livingston Island, Antarctica). *Catena* 149, 548–559. <https://doi.org/10.1016/j.catena.2016.07.011>.
- Parica, C.A., Salani, F.M., Vera, E., Remesal, M., Césari, S.N., 2007. Geología de la formación Cerro Negro (Cretácico) en la isla Livingston: aportes a su geocronología y contenido paleontológico. *Rev. Asoc. Geol. Argent.* 62, 553–567.
- Porter, S.C., 2000. Onset of neoglaciation in the southern hemisphere. *J. Quat. Sci.: Publ. Quat. Res. Assoc.* 15 (4), 395–408.
- Porter, S.C., Denton, G.H., 1967. Chronology of the neoglaciation in the North American cordillera. *Am. J. Sci.* 265 (3), 177–210.
- Pritchard, H.D., Ligtenberg, S.R.M., Fricker, H.A., Vaughan, D.G., van den Broeke, M.R., Padman, L., 2012. Antarctic ice-sheet loss driven by basal melting of ice shelves. *Nature* 484, 502–505. <https://doi.org/10.1038/nature10968>.
- Reilly, B.T., Natter, C.J., Brachfeld, S.A., 2016. Holocene glacial activity in Barilari Bay, west Antarctic Peninsula, tracked by magnetic mineral assemblages: linking ice, ocean, and atmosphere. *Geochem., Geophys., Geosyst.* 17 (11), 4553–4565. <https://doi.org/10.1002/2016GC006627>.
- Renssen, H., Seppä, H., Heiri, O., Rotche, D.M., Goosse, H., Fichfet, T., 2009. The spatial and temporal complexity of the Holocene thermal maximum. *Nat. Geosci.* 2 (6), 411. <https://doi.org/10.1038/NNGEO513>.
- Renssen, H., Seppä, H., Crosta, X., Goosse, H., Rotche, D.M., 2012. Global characterization of the Holocene thermal maximum. *Quat. Sci. Rev.* 48, 7–19. <https://doi.org/10.1016/j.quascirev.2012.05.022>.
- Roberts, S.J., Hodgson, D.A., Sterken, M., Whitehouse, P.L., Verleyen, E., Vyverman, W., Moreton, S.G., 2011. Geological constraints on glacio-isostatic adjustment models of relative sea-level change during deglaciation of Prince Gustav Channel, Antarctic Peninsula. *Quat. Sci.*
- Rothwell, R.G., Rack, F.R., 2006. *Reviews*, 30(25–26), 3603–3617. *New Techniques in Sediment Core Analysis: an Introduction*. Geological Society, vol. 267. Special Publications, London, pp. 1–29. <https://doi.org/10.1016/j.quascirev.2011.09.009> (1).
- Ruiz-Fernández, J., Oliva, M., 2016. Relative paleoenvironmental adjustments following deglaciation of the Byers peninsula (Livingston island, Antarctica). *Arctic Antarct. Alpine Res.* 48 (2), 345–359. <https://doi.org/10.1657/AAAR0015-014>.
- Ruiz-Fernández, J., Oliva, M., García-Hernández, C., 2016. Procesos geomorfológicos y formas del relieve en dos cuencas lacustres de la Península Byers (Isla Livingston, Antártida Marítima): implicaciones paleoambientales. *Polígonos. Rev. Geogr.* 28, 211–237.
- Sadatzki, H., Dokken, T.M., Berben, S.M., Muschitiello, F., Stein, R., Fahl, K., Jansen, E., 2019. Sea ice variability in the southern Norwegian Sea during glacial Dansgaard-Oeschger climate cycles. *Sci. Adv.* 5 (3) <https://doi.org/10.1126/sciadv.aau6174>.
- Sancho, L.G., Pintado, A., Navarro, F., Ramos, M., De Pablo, M.A., Blanquer, J.M., Green, T.G.A., 2017. Recent warming and cooling in the Antarctic Peninsula region has rapid and large effects on lichen vegetation. *Sci. Rep.* 7 (1), 5689. <https://doi.org/10.1038/s41598-017-05989-4>.
- Schäfer, J.M., Ivy-Ochs, S., Wieler, R., Leya, I., Baur, H., Denton, G.H., Schlüchter, C., 1999. Cosmogenic noble gas studies in the oldest landscape on earth: surface exposure ages of the Dry Valleys, Antarctica. *Earth Planet Sci. Lett.* 167 (3–4), 215–226. [https://doi.org/10.1016/S0012-821X\(99\)00029-1](https://doi.org/10.1016/S0012-821X(99)00029-1).
- Schimmelpfennig, I., Benedetti, L., Finkel, R., Pik, R., Blard, P.H., Bourlès, D., Burnard, P., Williams, A., 2009. Sources of in-situ <sup>36</sup>Cl in basaltic rocks. Implications for calibration of production rates. *Quat. Geochronol.* 4, 441–461. <https://doi.org/10.1016/j.quageo.2009.06.003>.
- Schimmelpfennig, I., Benedetti, L., Garreta, V., Pik, R., Blard, P.H., Burnard, P., Bourlès, D., Finkel, R., Ammon, K., Dunai, T., 2011. Calibration of cosmogenic <sup>36</sup>Cl production rates from Ca and K spallation in lava flows from Mt. Etna (38°N, Italy) and Payun Matru (36°S, Argentina). *Geochem. Cosmochim. Acta* 75, 2611–2632. <https://doi.org/10.1016/j.gca.2011.02.013>.
- Schimmelpfennig, I., Schaefer, J.M., Putnam, A.E., Koffman, T., Benedetti, L., Ivy-Ochs, S., Team, A., Schlüchter, C., 2014. <sup>36</sup>Cl production rate from K-spallation in the European Alps (Chironico landslide, Switzerland). *J. Quat. Sci.* 29, 407–413. <https://doi.org/10.1002/jqs.2720>.
- Schimmelpfennig, I., Tesson, J., Blard, P.H., Benedetti, L., Zakari, M., Balco, G., 2019. The CREP Chlorine-36 Exposure Age and Depth Profile Calculator. *GoldSchmidt*. Spain, Barcelona. <https://goldschmidtabstracts.info/2019/2996.pdf>.
- Sejrup, H.P., Seppä, H., McKay, N.P., Kaufman, D.S., Geirsdóttir, Á., de Vernal, A., Andrews, J.T., 2016. North Atlantic-Fennoscandian Holocene climate trends and mechanisms. *Quat. Sci. Rev.* 147, 365–378.
- Seong, Y.B., Owen, L.A., Lim, H.S., Yoon, H.I., Kim, Y., Lee, Y.I., Caffee, M.W., 2009. Rate of late quaternary ice-cap thinning on king George island, South Shetland islands, west Antarctica defined by cosmogenic <sup>36</sup>Cl surface exposure dating. *Boreas* 38 (2), 207–213. <https://doi.org/10.1111/j.1502-3885.2008.00069.x>.
- Serrano, E., Martínez De Pisón, E., López-Martínez, J., 1996. Periglacial and nival landforms and deposits. In: López-Martínez, J., Thomson, M.R.A., Thomson, J.W. (Eds.), *Geomorphological Map of Byers Peninsula, Livingston Island. BAS GEOMAP Series, Sheet 5-A, Scale 1:25 000. British Antarctic Survey, Cambridge*, pp. 28–34.
- Severinghaus, J.P., Brook, E., 1999. Abrupt climate change at the end of the last glacial period inferred from trapped air in polar ice. *Science* 286, 930–934.
- Shulmeister, J., Thackray, G.D., Rittenour, T.M., Fink, D., Patton, N.R., 2019. The timing and nature of the last glacial cycle in New Zealand. *Quat. Sci. Rev.* 206, 1–20.

- Simkins, L.M., Simms, A.R., DeWitt, R., 2013. Relative sea-level history of Marguerite Bay, Antarctic Peninsula derived from optically stimulated luminescence-dated beach cobbles. *Quat. Sci. Rev.* 77, 141–155. <https://doi.org/10.1016/j.quascirev.2013.07.027>.
- Simms, A.R., Milliken, K.T., Anderson, J.B., Wellner, J.S., 2011a. The marine record of deglaciation of the south Shetland islands, Antarctica since the last glacial maximum. *Quat. Sci. Rev.* 30 (13–14), 1583–1601. <https://doi.org/10.1016/j.quascirev.2011.03.018>.
- Simms, A.R., De Witt, R., Kouremenos, P., Drewry, A.M., 2011b. A new approach to reconstructing sea levels in Antarctica using optically stimulated luminescence of cobble surfaces. *Quat. Geochronol.* 6 (1), 50–60.
- Simms, A.R., Ivins, E.R., DeWitt, R., Kouremenos, P., Simkins, L.M., 2012. Timing of the most recent Neoglacial advance and retreat in the South Shetland Islands, Antarctic Peninsula: insights from raised beaches and Holocene uplift rates. *Quat. Sci. Rev.* 47, 41–55. <https://doi.org/10.1016/j.quascirev.2012.05.013>.
- Simms, A.R., Whitehouse, P.L., Simkins, L.M., Niold, G., DeWitt, R., Bentley, M.J., 2018. Late Holocene relative sea levels near Palmer Station, northern Antarctic Peninsula, strongly controlled by late Holocene ice-mass changes. *Quat. Sci. Rev.* 199, 49–59. <https://doi.org/10.1016/j.quascirev.2018.09.017>.
- Simonsen, M.F., Baccolo, G., Blunier, T., et al., 2019. East Greenland ice core dust record reveals timing of Greenland ice sheet advance and retreat. *Nat. Commun.* 10, 4494. <https://doi.org/10.1038/s41467-019-12546-2>.
- Singer, B.S., Jicha, B.R., Mochizuki, N., Coe, R.S., 2019. Synchronizing volcanic, sedimentary, and ice core records of Earth's last magnetic polarity reversal. *Sci. Adv.* 5 (8) <https://doi.org/10.1126/sciadv.aaw4621> eaaw4621.
- Smellie, J.L., Davies, R.E.S., Thomson, M.R.A., 1980. Geology of a mesozoic intra-arc sequence on Byers peninsula, Livingston island, South Shetland islands. *Br. Antarct. Surv. Bull.* 50, 55–76.
- Solomina, O.N., Bradley, R.S., Hodgson, D.A., Ivy-Ochs, S., Jomelli, V., Mackintosh, A.N., Young, N.E., 2015. Holocene glacier fluctuations. *Quat. Sci. Rev.* 111, 9–34. <https://doi.org/10.1016/j.quascirev.2014.11.018>.
- Stolper, D., Bender, M., Dreyfus, G., Yan, Y., Higgins, J.A., 2016. Pleistocene ice core record of atmospheric O<sub>2</sub> concentrations. *Science* 353, 1427–1430.
- Stone, J.O., 2000. Air pressure and cosmogenic isotope production. *J. Geophys. Res. Solid Earth* 105, 23753–23759. <https://doi.org/10.1029/2000JB900181>.
- Stone, J.O., Fifield, L.K., Vasconcelos, P., 2005. Terrestrial Chlorine-36 Production from Spallation of Iron. In: Abstracts of 10th International Conference on Accelerator Mass Spectrometry, September 5–10. Berkeley University, Berkeley, CA.
- Storey, B.C., Fink, D., Hood, D., Joy, K., Shulmeister, J., Riger-Kusk, M., Stevens, M.I., 2010. Cosmogenic nuclide exposure age constraints on the glacial history of the Lake Wellman area, Darwin Mountains, Antarctica. *Antarct. Sci.* 22 (6), 603–618. <https://doi.org/10.1017/S0954102010000799>.
- Strelin, J., Sone, T., Mori, J., Torielli, C., Nakamura, T., 2006. New data related to Holocene landform development and climatic change from James Ross island, antarctic peninsula. In: Fütterer, D., Damaske, D., Kleinschmidt, G., Miller, H., Tessensohn, F. (Eds.), *Antarctica: Contributions to Global Earth Sciences*. Springer-Verlag, New York, pp. 455–460.
- Sugden, D.E., Clapperton, C.M., 1986. Glacial history of the antarctic peninsula and South Georgia. *South Afr. J. Sci.* 82 (9), 508–509.
- Sugden, D.E., John, B.S., 1973. The ages of glacier fluctuations in the South Shetland Islands, Antarctica. In: van Zinderen Bakker, E.M. (Ed.), *Palaeoecology of Africa, the Surrounding Islands and Antarctica*, vol. 8, pp. 141–159 (Balkema, Cape Town).
- Toro, M., Granados, I., Pla, S., Giralt, S., Antoniades, D., Galán, L., Appleby, P.G., 2013. Chronostratigraphy of the sedimentary record of limnopol lake, Byers peninsula, Livingston island, Antarctica. *Antarct. Sci.* 25 (2), 198–212. <https://doi.org/10.1017/S0954102012000788>.
- Turner, J., Colwell, S.R., Marshall, G.J., Lachlan-Cope, T.A., Carleton, A.M., Jones, P.D., lagovkina, S., 2005. Antarctic climate change during the last 50 years. *Int. J. Climatol.* 25 (3), 279–294. <https://doi.org/10.1002/joc.1130>.
- Turner, J., Lu, H., White, I., King, J.C., Phillips, T., Hosking, J.S., Deb, P., 2016. Absence of 21st century warming on Antarctic Peninsula consistent with natural variability. *Nature* 535 (7612), 411. <https://doi.org/10.1038/nature18645>.
- Uppala, S.M., Källberg, P.W., Simmons, A.J., Andrae, U., da Costa Bechtold, V., Fiorino, M., Gibson, J.K., Haseler, J., Hernandez, A., Kelly, G.A., Li, X., Onogi, K., Saarinen, S., Sokka, N., Allan, R.P., Andersson, E., Arpe, K., Balmaseda, M.A., Beljaars, A.C.M., van de Berg, L., Bidlot, J., Bormann, N., Caires, S., Chevallier, F., Dethof, A., Dragosavac, M., Fisher, M., Fuentes, M., Hagemann, S., Hólm, E., Hoskins, B.J., Isaksen, I., Janssen, P.A.E.M., Jenne, R., McNally, A.P., Mahfouf, J.F., Morcrette, J.J., Rayner, N.A., Saunders, R.W., Simon, P., Sterl, A., Trenberth, K.E., Untch, A., Vasiljevic, D., Viterbo, P., Woollen, J., 2005. The ERA-40 re-analysis. *Q. J. R. Meteorol. Soc.* 131, 2961–3012. <https://doi.org/10.1256/qj.04.176>.
- Vaughan, D.G., Doake, C.S.M., 1996. Recent atmospheric warming and retreat of ice shelves on the Antarctic Peninsula. *Nature* 379, 328–331.
- Vaughan, D.G., Marshall, G., Connolley, W.M., Parkinson, C., Mulvaney, R., Hodgson, D.A., King, J.C., Pudsey, C.J., Turner, J., Wolff, E., 2003. Recent rapid regional climate warming on the Antarctic Peninsula. *Climatic Change* 60, 243–274.
- Vera, M., 2013. Distribution and reproductive capacity of *deschampsia* Antarctica and *Colobanthus quitensis* on Byers peninsula, Livingston island, South Shetland islands, Antarctica. *Antarct. Sci.* 25 <https://doi.org/10.1017/S0954102012000995>.
- Watcham, E.P., Bentley, M.J., Hodgson, D.A., Roberts, S.J., Fretwell, P.T., Lloyd, J.M., Moreton, S.G., 2011. A new Holocene relative sea level curve for the South Shetland Islands, Antarctica. *Quat. Sci. Rev.* 30 (21–22), 3152–3170. <https://doi.org/10.1016/j.quascirev.2011.07.021>.
- White, D.A., Fink, D., Gore, D.B., 2011. Cosmogenic nuclide evidence for enhanced sensitivity of an East Antarctic ice stream to change during the last deglaciation. *Geology* 39 (1), 23–26. <https://doi.org/10.1130/G31591.1>.
- Yoo, K.C., Yoon, H.I., Kim, J.K., Khim, B.K., 2009. Sedimentological, geochemical and palaeontological evidence for a neoglacial cold event during the late Holocene in the continental shelf of the northern South Shetland Islands, West Antarctica. *Polar Res.* 28 (2), 177–192. <https://doi.org/10.1111/j.1751-8369.2009.00109.x>.
- Yoon, H.I., Yoo, K.C., Bak, Y.S., Lim, H.S., Kim, Y., Lee, J.I., 2010. Late Holocene cyclic glaciomarine sedimentation in a subpolar fjord of the South Shetland Islands, Antarctica, and its paleoceanographic significance: sedimentological, geochemical, and paleontological evidence. *Bulletin* 122 (7–8), 1298–1307.
- Zale, R., Karlén, W., 1989. lake sediment cores from the antarctic peninsula and surrounding islands. *Geografiska annaler: series A. Phys. Geogr.* 71 (3–4), 211–220.
- Mulvaney, R., Abram, N.J., Hindmarsh, R.C., Arrowsmith, C., Fleet, L., Triest, J., Foord, S., 2012. Recent Antarctic Peninsula warming relative to Holocene climate and ice-shelf history. *Nature* 489 (7414), 141. <https://doi.org/10.1038/nature11391>.
- Shevenell, A.E., Ingalls, A.E., Domack, E.W., Kelly, C., 2011. Holocene Southern Ocean surface temperature variability west of the Antarctic Peninsula. *Nature* 470 (7333), 250. <https://doi.org/10.1038/nature09751>.